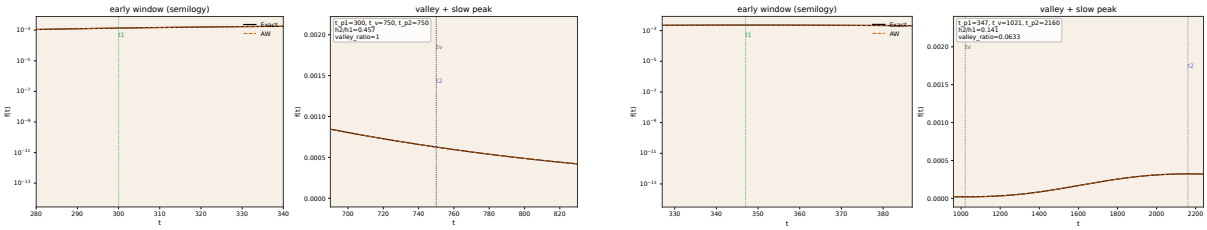
Bimodal first-passage times on a 2D $N \times N$ lattice with **reflecting boundaries**

Summary and Key Figures

- **Bimodality persists under fully reflecting boundaries**: we keep eight representative cases R1 (geometric detour), R7 (semipermeable pore + detour), C3 (active transport track), R6 (door array), NB4 (perimeter conveyor template), NB5 (conveyor + global bias), and S1/S2 (soft two-track constructions with zero internal barriers/doors), all showing clear bimodal FPTs.
- **Geometric vs dynamical slow channels**: R1/R7/C3 use "short corridor + long detour" geometry with a local pore/track; R6 delays by a door array; NB4/NB5 use a clockwise boundary belt vs a short counterflow path; S1/S2 create soft corridors via sticky + local arrows without hard walls.
- **Deep valley with minimal structure**: NB4/NB5 modify only the boundary (sticky + clockwise bias), while S1/S2 avoid internal barrier/door entirely yet still reach valley ratio ≤ 0.07.
- **Quantified bimodality**: peak/valley metrics and MC fast-channel weights are summarized in Table 2; AW errors reach the 10^{-14} level (Table 5).
- **AW vs exact validation**: for $t \leq t_{\max}^{\mathrm{AW}}$, AW inversion matches exact recursion and agrees with the MC overlays.



(a) R1 peak–valley zoom (b) R6 peak–valley zoom

Figure 1: Bimodality examples under reflecting boundaries (R1 and R6).

case	N	q	g_x	g_y	boundary	(start, target)
R1	60	0.8	-0.20	0.00	reflecting	(10,30)→(50,30)
R7	60	0.8	-0.20	0.00	reflecting	(10,30)→(50,30)
C3	60	0.8	-0.15	0.00	reflecting	(10,30)→(50,30)
R6	60	0.8	0.00	0.00	reflecting	(10,30)→(50,30)
NB4	60	0.8	0.00	0.00	reflecting	(12,60)→(10,60)
NB5	60	0.8	-0.10	0.00	reflecting	(12,60)→(10,60)
S1	60	0.8	0.00	0.00	reflecting	(10,30)→(50,30)
S2	60	0.8	0.00	0.00	reflecting	(10,30)→(50,30)

Table 1: Core parameters for the representative reflecting-boundary constructions.

case	t_{p1}	t_v	t_{p2}	peak ratio	valley ratio	P_{fast} (MC)
R1	136	269	424	0.451	0.035	0.321
R7	140	280	428	0.294	0.066	0.248
C3	160	388	702	0.231	0.022	0.293
R6	347	1021	2160	0.141	0.063	0.498
NB4	6	389	642	0.932	0.062	0.104
NB5	6	379	621	0.930	0.009	0.024
S1	47	240	363	0.641	0.037	0.127
S2	48	274	462	0.647	0.061	0.171

Table 2: Peak/valley metrics and MC fast-channel weights for the representative constructions (absorption probability is near 1 at the truncation time).

Parameter Table

Bimodality Metrics

1 Model Definition and Coordinate Convention

The state space is $\{1,\dots,N\}\times\{1,\dots,N\}$. The walker is at (x,y) and the target (x_t,y_t) is absorbing. One-step transition probabilities are

$$p_{\text{left}} = \frac{q}{4}(1+g_x), \quad p_{\text{right}} = \frac{q}{4}(1-g_x), \tag{1}$$

$$p_{\text{down}} = \frac{q}{4}(1+g_y), \quad p_{\text{up}} = \frac{q}{4}(1-g_y), \tag{2}$$

$$p_{\text{stay}} = 1-q. \tag{3}$$

We adopt the convention "y increases downward", so $g_y>0$ means downward drift. This report uses **fully reflecting boundaries**: out-of-boundary probabilities are added back to p_{stay}. From Eq.(1), $g_x>0$ increases p_{left} and decreases p_{right}, so we define $g_x>0$ as a **leftward** global bias ($g_x<0$ is rightward).

Local heterogeneities (combinations).

- local bias (arrow): multiply p_{stay} by $(1-\delta)$ and add $\Delta=\delta p_{\text{stay}}$ to the arrow direction; other directions stay unchanged.
- sticky site: scale the move rate to $q_{\text{site}}=\text{factor}\cdot q$; p_{stay} increases accordingly.
- barrier: a reflecting wall adds its probability back to stay; a door passes with p_{pass} and reflects with $1-p_{\text{pass}}$.

2 How to Read the Figures

Fig. 2 gives the unified symbol legend: red squares are starts, blue diamonds are targets; thick solid lines are reflecting walls, dashed lines are doors (labeled by p_{pass}), translucent shading is sticky regions; red arrows are local bias sites; large arrows outside the grid indicate the global drift and (g_x, g_y). For readability, environment schematics, $P(n,t)$ slices, multiscale FPT plots, peak–valley zooms, diagnostics, and channel decompositions are shown as separate figures.



Figure 2: Symbol legend.

3 FPT primer: definition, intuition, and three methods

Definition and intuition The first-passage time (FPT) is

$$\tau = \inf\{t \geq 1 : X_t = (x_t, y_t)\},$$

with PMF $f(t) = \Pr(\tau = t)$, CDF $F(t) = \Pr(\tau \leq t)$, and survival

$$S(t) = \Pr(\tau > t) = 1 - F(t).$$

Intuitively, $f(t)$ is the probability of first hitting the target *exactly* at step t. The bimodality in this report is simply two visible local maxima of $f(t)$ at early and late times.

Three ways to compute $f(t)$ (plain-language) We overlay three estimates of $f(t)$ throughout the report:

- **Exact recursion (deterministic)**: build the transient submatrix Q, then push the distribution forward one step at a time:

$$p_{t+1} = Qp_t, \qquad f(t) = r^\top p_t, \quad t \geq 1,$$

  where r is the absorption flux vector. This is the step-by-step, deterministic baseline.
- **AW inversion (generating-function inversion)**: compute the generating function $\tilde{f}(z)$ (from the propagator and defect formula), then invert via Abate–Whitt:

$$f(t) \approx r^{-t} \frac{1}{m} \sum_{k=0}^{m-1} \tilde{f}(z_k) e^{-2\pi i k t/m}.$$

  Think of it as "work in the z-domain, then invert back to time".
- **Monte Carlo (MC)**: simulate many random walks, then histogram the hitting times. This is flexible but noisy in the tail unless you run many samples.

AW vs Exact (beginner-friendly comparison)

- **Accuracy**: Exact is deterministic; AW can be as accurate as Exact with proper parameters; MC is statistical with error $\propto 1/\sqrt{N}$.

- **Speed and use cases**: Exact is good for moderate sizes and finite $t_{\max}$; AW is efficient once $\tilde{f}(z)$ is available but can be slowed by solving a linear system at each z_k when many defects exist; MC is best for quick sanity checks or very large systems where exact state-space recursion is too expensive.
- **What we do here**: Exact is the baseline, AW is used to validate inversion accuracy, and MC provides a stochastic cross-check plus channel classification intuition.

4 Analytical derivation: from defect-free propagator to time-domain FPT

This section provides a unified derivation chain: *defect-free propagator → defect propagator → FPT generating function → AW inversion*. The constructions in this report fit this framework.

4.1 Matrix form and generating function

Let A be the transition matrix for the non-absorbing system, with $A_{v,u} = \Pr(u \to v)$ so columns sum to 1 and $\mathbf{p}_{t+1} = A\mathbf{p}_t$. The propagator satisfies

$$P_{n_0}(n,t) = \mathbf{e}_n^\top A^t \mathbf{e}_{n_0}, \qquad \tilde{\mathbf{P}}(z) = \sum_{t\geq 0} A^t z^t = (I - zA)^{-1}, \tag{4}$$

so

$$\tilde{P}_{n_0}(n,z) = \mathbf{e}_n^\top (I - zA)^{-1} \mathbf{e}_{n_0}. \tag{5}$$

We now give the spectral form of A and the defect update formula to obtain $\tilde{P}$ for any configuration.

4.2 Spectral decomposition of the defect-free propagator (reflecting)

Write the 2D update as the sum of two 1D operators (along x and y). Let $\{\lambda_k^{(\mathrm{ref})}, h_k^{(\mathrm{ref})}\}$ be eigenpairs of the 1D step matrix. Define

$$s_k^{(\mathrm{ref})} = q\left(\lambda_k^{(\mathrm{ref})} - 1\right), \qquad \Lambda_{k_1,k_2} = 1 + \frac{s_{k_1}^{(\mathrm{ref})} + s_{k_2}^{(\mathrm{ref})}}{2}. \tag{6}$$

Then the 2D defect-free propagator (Eq.(33) in PRE 102, 062124) is

$$P_{n_0}^{(\mathrm{ref})}(n,t) = \sum_{k_1}\sum_{k_2} h_{k_1}^{(\mathrm{ref})}(x,x_0)\, h_{k_2}^{(\mathrm{ref})}(y,y_0)\, \Lambda_{k_1,k_2}^t. \tag{7}$$

The z-transform is

$$\tilde{P}_{n_0}^{(\mathrm{ref})}(n,z) = \sum_{k_1}\sum_{k_2} \frac{h_{k_1}^{(\mathrm{ref})}(x,x_0)\, h_{k_2}^{(\mathrm{ref})}(y,y_0)}{1 - z\Lambda_{k_1,k_2}}. \tag{8}$$

Reflecting boundary Let $p_\ell = (1+g)/2,\ p_r = (1-g)/2,\ \rho = p_r/p_\ell$. A similarity transform symmetrizes the 1D operator, giving

$$\lambda_0^{(\mathrm{ref})} = 1, \quad \lambda_k^{(\mathrm{ref})} = 2\sqrt{p_\ell p_r}\cos\frac{k\pi}{N}\ (k \geq 1), \quad h_k^{(\mathrm{ref})}(x,x_0) = u_k(x)u_k(x_0)\sqrt{\frac{\pi_x}{\pi_{x_0}}}, \tag{9}$$

where $\pi_x \propto \rho^x$ is the stationary distribution and u_k are orthogonal cosine modes (matching PRE Eq.(22)–(23)).

4.3 Determinant formula for defect propagator

Write the defect as a matrix perturbation $\underline{X} = \underline{B} - \underline{A}$. For each directed edge $(u_i \to v_i)$, define

$$\eta_{u_i,v_i} = X_{v_i,u_i} = B_{v_i,u_i} - A_{v_i,u_i}. \tag{10}$$

Define the difference propagator

$$\tilde{P}^e_{\langle u-v\rangle}(n,z) = \tilde{P}^e_u(n,z) - \tilde{P}^e_v(n,z). \tag{11}$$

Then the inert-heterogeneity formula (2311.00464v2) gives

$$\tilde{P}_{n_0}(n,z) = \tilde{P}^e_{n_0}(n,z) - 1 + \frac{\det[H(n,n_0;z)]}{\det[H(z)]}, \tag{12}$$

with

$$H_{ij}(z) = -\frac{\delta_{ij}}{z} + \eta_{u_j,v_j}\,\tilde{P}^e_{\langle u_j-v_j\rangle}(u_i,z) - \eta_{v_j,u_j}\,\tilde{P}^e_{\langle u_j-v_j\rangle}(v_i,z), \tag{13}$$

$$H(n,n_0;z)_{ij} = H_{ij}(z) - \tilde{P}^e_{\langle u_j-v_j\rangle}(n,z)\left[\eta_{u_i,v_i}\tilde{P}^e_{n_0}(u_i,z) - \eta_{v_i,u_i}\tilde{P}^e_{n_0}(v_i,z)\right]. \tag{14}$$

In numerical implementations, we solve the equivalent linear system for stability (by Cramer equivalence). The linear-algebra form reads

$$b_j(n,z) = \tilde{P}^e_{u_j}(n,z) - \tilde{P}^e_{v_j}(n,z), \tag{15}$$

$$a_i(n_0,z) = \eta_{u_i,v_i}\tilde{P}^e_{n_0}(u_i,z) - \eta_{v_i,u_i}\tilde{P}^e_{n_0}(v_i,z), \tag{16}$$

$$H_{ij}(z) = -\frac{\delta_{ij}}{z} + \eta_{u_j,v_j}\,b_j(u_i,z) - \eta_{v_j,u_j}\,b_j(v_i,z), \tag{17}$$

so that

$$\tilde{P}_{n_0}(n,z) = \tilde{P}^e_{n_0}(n,z) - \mathbf{b}(n,z)^\top H(z)^{-1}\mathbf{a}(n_0,z). \tag{18}$$

Defect mapping

- local bias: reduce the self-loop and add probability to the arrow direction, equivalent to $(u \to v)$ with $\eta_{u,v} = +\Delta$, plus a compensation term for $(u \to u)$ to keep column sums at 1.
- door/permeable barrier: crossing the door multiplies by p_{pass}; both $(u \to v)$ and $(v \to u)$ have $\eta_{u,v} = (p_{\text{pass}} - 1)P^{\text{base}}_{u\to v}$.
- sticky: multiply all outgoing edges by α; each outgoing edge $(u \to n)$ has $\eta_{u,n} = (\alpha-1)P^{\text{base}}_{u\to n}$, with a compensation term added to $(u \to u)$ to keep column sums at 1.

feature	rule (example $u \to v$)	corresponding $\lambda_{u,v}$
local bias	$p_{u\to v} = p^0_{u\to v} + \Delta$	$-\Delta/p^0_{u\to v}$
sticky	$p_{u\to v} = \alpha p^0_{u\to v}$	$1-\alpha$
barrier	$p_{u\to v} = 0$	1
door	$p_{u\to v} = p_{\text{pass}} p^0_{u\to v}$	$1 - p_{\text{pass}}$

Table 3: Mapping from features to λ ($\eta_{u,v} = -\lambda_{u,v}p^0_{u\to v}$).

4.4 FPT generating function and AW inversion

Consider the master equation with an absorbing state:

$$\mathbf{p}_{t+1} = P\,\mathbf{p}_t, \qquad \mathbf{p}_0 = \mathbf{e}_{n_0}, \tag{19}$$

with z-transform $\tilde{\mathbf{p}}(z) = \sum_{t\geq 0} \mathbf{p}_t z^t$ giving

$$\tilde{\mathbf{p}}(z) = (I - zP)^{-1}\mathbf{p}_0. \tag{20}$$

Let the cumulative arrival probability be $F(t) = \mathbf{e}_{n_t}^\top \mathbf{p}_t$, then

$$\tilde{F}(z) = \mathbf{e}_{n_t}^\top (I - zP)^{-1}\mathbf{p}_0. \tag{21}$$

With $f(t) = F(t) - F(t-1)$ (take $F(-1) = 0$), the PMF generating function is

$$\tilde{f}(z) = (1-z)\tilde{F}(z) = (1-z)\,\mathbf{e}_{n_t}^\top (I - zP)^{-1}\mathbf{p}_0. \tag{22}$$

We keep both notations: $\tilde{F}$ for the CDF generating function and $\tilde{f}$ for the PMF generating function (used in AW inversion). The exact recursion in time domain is

$$f(t) = r^\top Q^{t-1} p_0, \quad t \geq 1, \tag{23}$$

so the generating function is

$$\tilde{f}(z) = \sum_{t\geq 1} f(t) z^t = z\, r^\top (I - zQ)^{-1} p_0. \tag{24}$$

By the renewal relation,

$$\tilde{f}_{n_0 \to n_t}(z) = \frac{\tilde{P}_{n_0}(n_t, z)}{\tilde{P}_{n_t}(n_t, z)}, \tag{25}$$

which is equivalent to the transient-matrix formulation above. The Abate–Whitt (AW) inversion is

$$f(t) \approx r^{-t} \frac{1}{m} \sum_{k=0}^{m-1} \tilde{f}(z_k)\, e^{-2\pi i k t/m}, \qquad z_k = r\, e^{2\pi i k/m}, \quad t = 1, \ldots, t_{\max}^{\mathrm{AW}}. \tag{26}$$

We set $m = \mathrm{pow2}(\mathrm{oversample} \cdot (t_{\max}^{\mathrm{AW}} + 1))$ and $r^m = 10^{-\mathrm{r_pow10}}$ as in the repository.

Implementation (Algorithm box)

1. Build the spectral decomposition of A (reflecting boundaries) to obtain $\tilde{P}^e(n, z)$.
2. Construct $H(z)$ and vectors $\mathbf{a}, \mathbf{b}$ from the defect list, solve the linear system for $\tilde{P}(n, z)$.
3. Compute $\tilde{f}(z) = \tilde{P}_{n_0}(n_t, z)/\tilde{P}_{n_t}(n_t, z)$ via the renewal formula.
4. Sample $z_k = re^{2\pi i k/m}$ and perform AW inversion to obtain $f(t)$.
5. Compare with exact recursion/MC and record metrics in JSON.

4.5 AW vs exact recursion: principles and speed

Principles (with formulas) Let Q be the transient submatrix, r the absorption vector, and p_0 the initial distribution. Exact recursion uses the time-domain update

$$p_{t+1} = Qp_t, \qquad f(t) = r^\top p_t, \quad t \geq 1,$$

equivalently

$$f(t) = r^\top Q^{t-1} p_0, \qquad F(t) = 1 - \mathbf{1}^\top Q^t p_0.$$

For a given $t_{\max}$, this is deterministic and exact up to floating-point roundoff. AW works in the z domain: first form

$$\tilde{f}(z) = z\, r^\top (I - zQ)^{-1} p_0 = \frac{\tilde{P}_{n_0}(n_t, z)}{\tilde{P}_{n_t}(n_t, z)},$$

then extract coefficients via Cauchy inversion:

$$f(t) = \frac{1}{2\pi i} \oint_{|z|=r} \frac{\tilde{f}(z)}{z^{t+1}}\, dz \approx r^{-t} \frac{1}{m} \sum_{k=0}^{m-1} \tilde{f}(z_k) e^{-2\pi i k t/m}.$$

Complexity and suitability Exact recursion costs $O(T|E|)$ time ($T = t_{\max}$, $|E|$ nonzero transitions) and $O(|E|)$ memory, and is robust for medium-size parameter scans. AW solves an $M \times M$ system for each z (with M defects), giving $O(mM^3)$ overall; the FFT part $O(m \log m)$ is typically negligible, and AW becomes attractive only when M is small. AW is trivially parallel across z_k, while exact recursion is sequential but simple and numerically stable.

Accuracy notes Exact recursion is deterministic for the chosen $t_{\max}$ (errors are only floating-point roundoff), so we treat it as the baseline. AW is a numerical inversion; errors come from finite m, the choice of r, and conditioning of the linear solve for $\tilde{f}(z)$. Increasing m or tuning r improves accuracy. In this report, AW vs exact L^1 errors are $\sim 10^{-14}$ (Table 5), so both are numerically accurate for our cases.

Benchmark setup We benchmark R1/R7/C3/R6/NB4/NB5 with their native $t_{\max}$. AW uses oversample=4 and r_pow10=12, giving $m = 8192/16384/65536/131072$. To avoid the full AW runtime, we time $n_z = 32$ samples and estimate

$$t_{\mathrm{AW}} \approx t_{\mathrm{setup}} + (m/n_z)\, t_{\mathrm{eval}} + t_{\mathrm{FFT}}.$$

We also include a low-defect control S0 (full grid, one sticky + one door; $M = 9$), where the full AW runtime is feasible. Parameters are $N = 30$, start=(1,15), target=(30,15), $g_x = -0.4$, with sticky$(15, 15, \alpha = 0.1)$ and door$(20, 15) \leftrightarrow (21, 15)$ at $p_{\mathrm{pass}} = 0.05$. The script is `code/benchmark_aw_exact.py` (single-thread), and the results are in Table 4.

case	$t_{\max}$	M	Exact (s)	AW-inv (ms)	AW-total (s)
R1	1500	973	0.057	4.71	633 (10.6 min)
R7	2000	754	0.080	0.23	314 (5.2 min)
C3	3000	1004	0.106	0.45	1483 (24.7 min)
R6	12000	988	0.421	2.02	4862 (81.0 min)
NB4	20000	936	0.692	3.91	16786 (279.8 min)
NB5	20000	936	0.698	4.76	15946 (265.8 min)
S0	5000	9	0.056	0.97	1.44 (full AW)

Table 4: Runtime comparison between AW and exact recursion (M is the defect count; R1/R7/C3/R6/NB4/NB5 use estimated AW totals, S0 uses full AW runtime).

Takeaways (speed-first) For corridor/door constructions ($M \approx 7.5 \times 10^2$–$10^3$), exact recursion finishes in 0.06–0.70 s for $t_{\max} \le 2 \times 10^4$, while AW totals are 5–280 min, dominated by the per-z linear solves. Even small corridors like R7 ($M = 754$) and C3 ($M = 1004$) still yield 5.2 min and 24.7 min estimated AW totals, although AW inversion itself remains 0.23–4.76 ms. In S0 ($M = 9$), the full AW runtime is 1.44 s, but exact is still faster (0.056 s); AW would need fewer defects or accelerated linear solves to win. For scans or moderate $t_{\max}$, exact recursion is the practical choice; AW is preferable only when defects are few and long tails are needed.

5 Numerical Baseline: Exact/flux recursion and MC

Exact recursion on the transient space computes $f(t) = r^\top Q^{t-1} p_0$ (Eq. 23), and is used as a deterministic baseline. We overlay AW inversion and MC histograms in the multiscale FPT plots (Fig. 7, 15, 23, 31, 39, 47, 55, 63). MC trajectories are also classified into "fast/slow channels" to interpret bimodality.

Peak–valley metrics On the smoothed $f(t)$, identify two main peaks at t_{p1}, t_{p2} and the minimum between them at t_v. Define

$$h_1 = f(t_{p1}), \quad h_2 = f(t_{p2}), \quad \text{peak ratio} = \frac{\min(h_1, h_2)}{\max(h_1, h_2)}, \quad \text{valley ratio} = \frac{f(t_v)}{\min(h_1, h_2)}. \tag{27}$$

We use a smoothing window of 9; metrics and channel weights are generated by the same script and saved in metrics JSON.

case	L^1 error	L^∞ error
R1	2.55×10^{-15}	2.88×10^{-17}
R7	1.59×10^{-14}	1.10×10^{-16}
C3	4.93×10^{-15}	2.31×10^{-17}
R6	6.77×10^{-15}	1.32×10^{-17}
NB4	3.11×10^{-15}	3.12×10^{-18}
NB5	2.53×10^{-15}	2.53×10^{-18}
S1	3.08×10^{-14}	9.22×10^{-17}
S2	2.21×10^{-14}	6.32×10^{-17}

Table 5: AW inversion vs exact recursion errors for $t \le t_{\max}^{\mathrm{AW}}$ (L^1 and L^∞).

These errors confirm that AW accurately reproduces exact recursion over the inversion window and aligns with the MC overlays.

6 Selected Reflecting-Boundary Constructions

We highlight eight representative constructions (R1, R7, C3, R6, NB4, NB5, S1, S2) in the main text.

6.1 R1: short corridor vs top U-shaped detour

This is the simplest geometric two-channel construction: the bottom corridor is fast, the U-shaped detour is slow.

Configuration Card $N = 60$, $q = 0.8$, $g = (-0.20, 0)$ with reflecting boundaries; start=(10,30), target=(50,30). The reachable set is the main corridor $y = 30$, $x = 10..50$ plus a U-shaped detour (left column $x = 10$, $y = 1..30$, top edge $y = 1$, $x = 10..50$, right column $x = 50$, $y = 1..30$), with reflecting walls elsewhere. Local bias is rightward on the main corridor ($\delta = 0.95$), $\delta = 0.6$ at the junction $(10, 30)$, and follows the detour's up/right/down directions with $\delta = 0.95$. The channel rule treats any visit to the detour (upper segments of $x = 10$ or $x = 50$, or the top edge $y = 1$) as slow; otherwise the path stays on $y = 30$ and is fast. Metrics: $t_{p1} = 136$, $t_v = 269$, $t_{p2} = 424$; peak ratio= 0.451; valley ratio= 0.035; $P_{\mathrm{fast}} = 0.321$.

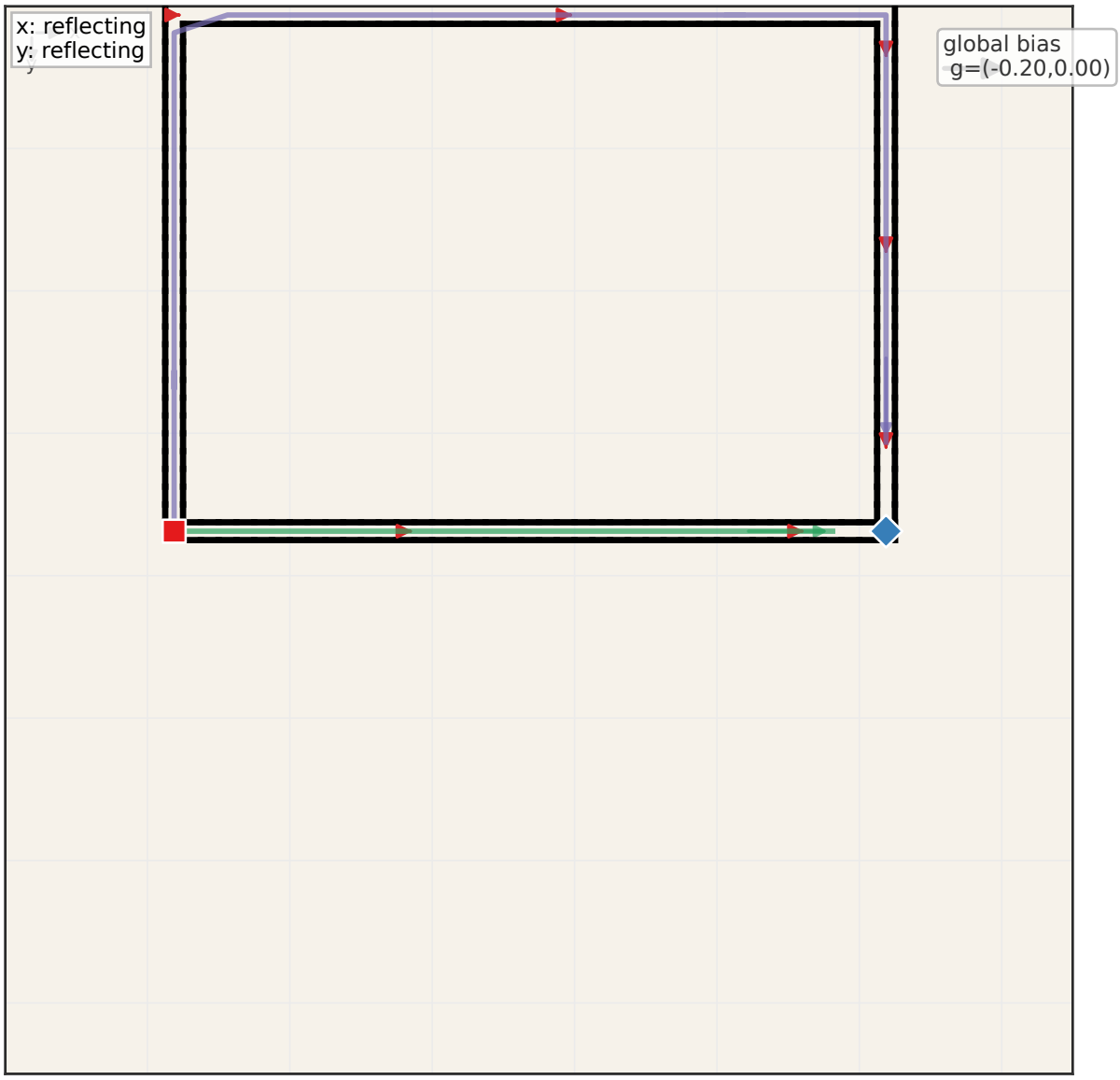


Figure 3: R1: environment schematic. Symbols follow Fig. 2.

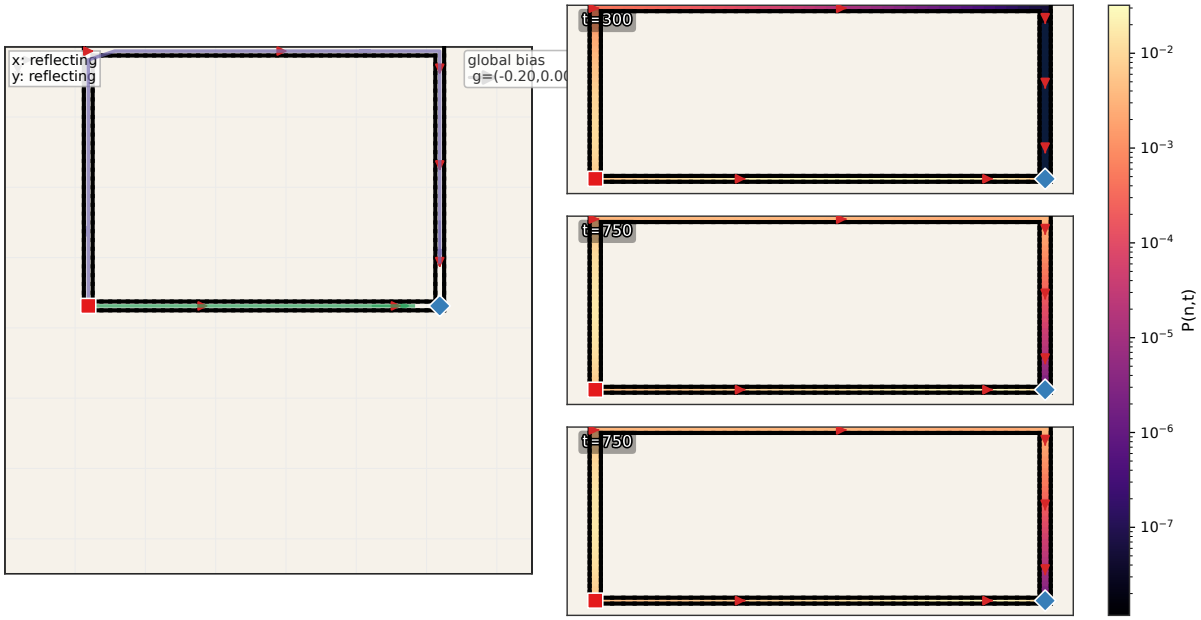


Figure 4: R1: environment and $P(n,t)$ slices at t_{p1}, t_v, t_{p2}.

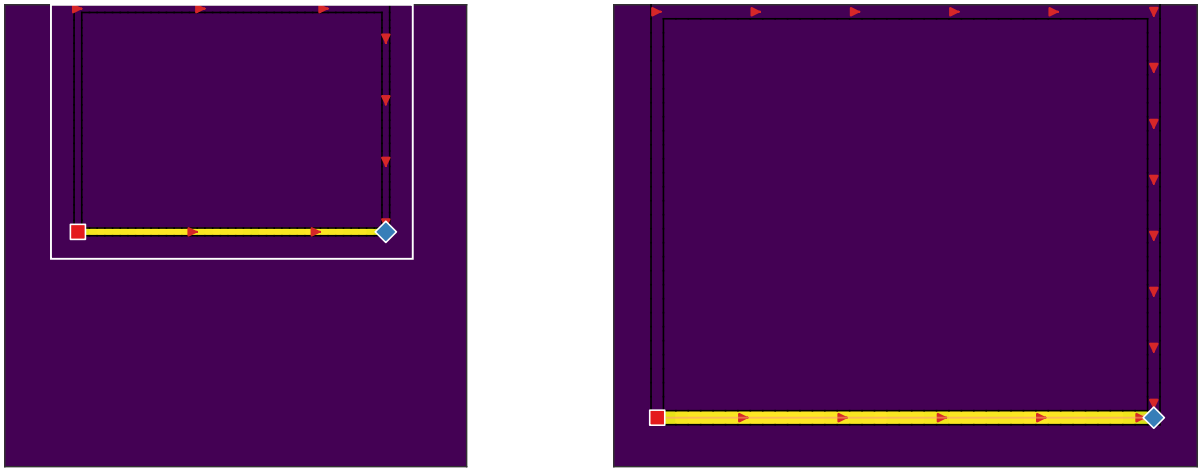


Figure 5: R1: fast-channel path density + representative paths (full + ROI).

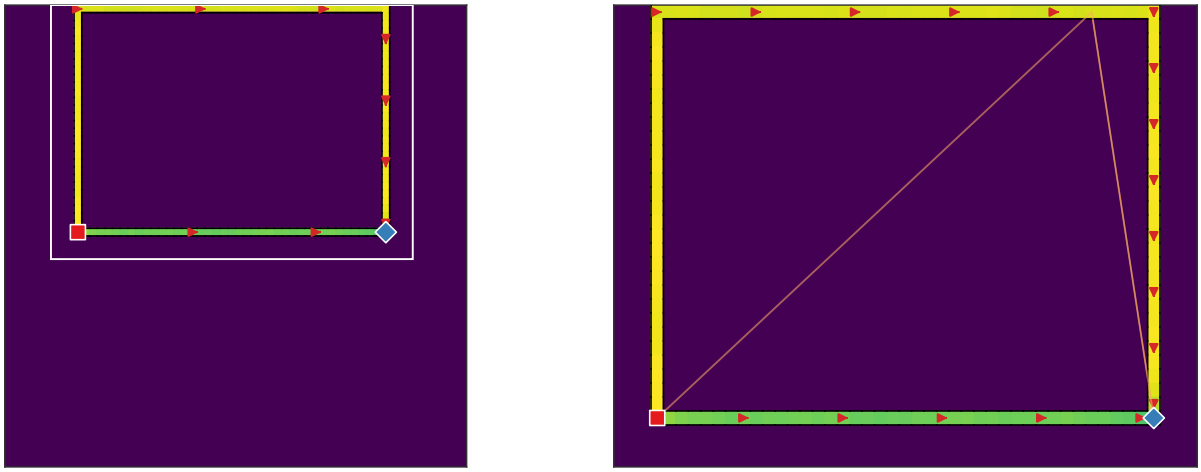


Figure 6: R1: slow-channel path density + representative paths (full + ROI).

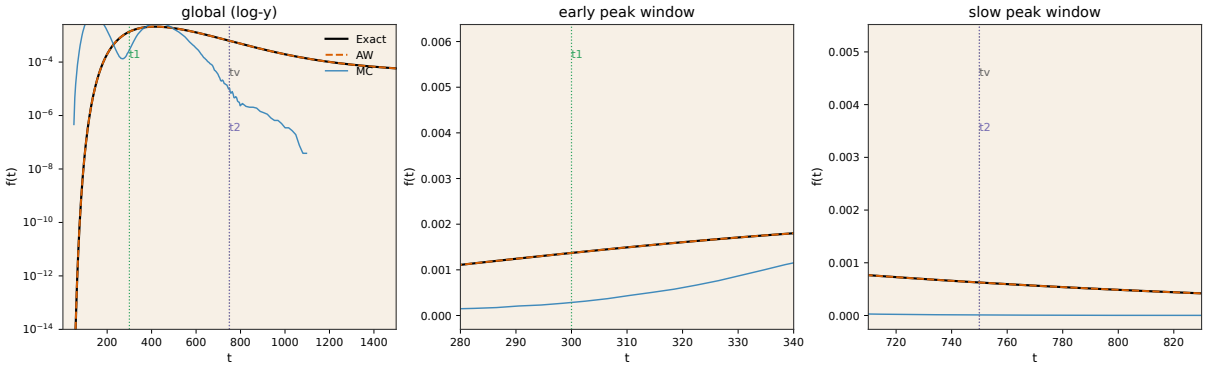


Figure 7: R1: multiscale FPT plot (Exact/AW/MC overlay).

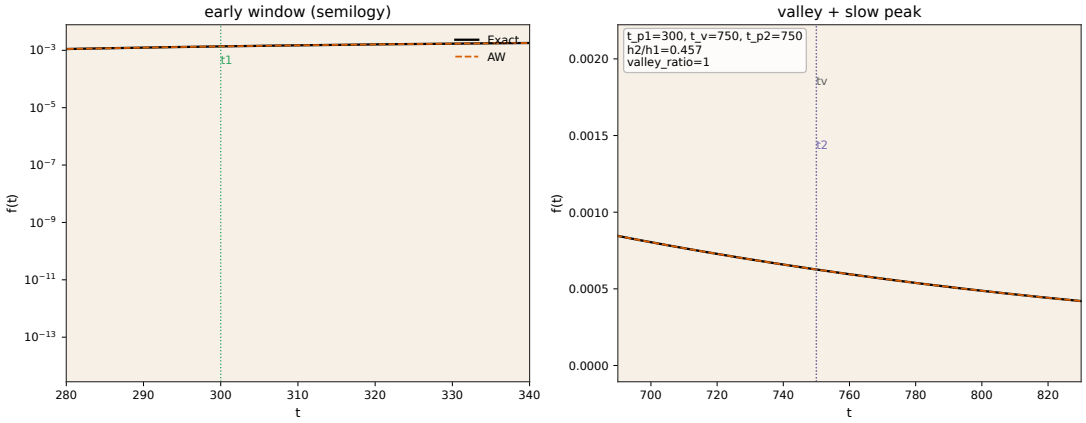


Figure 8: R1: peak–valley zoom.

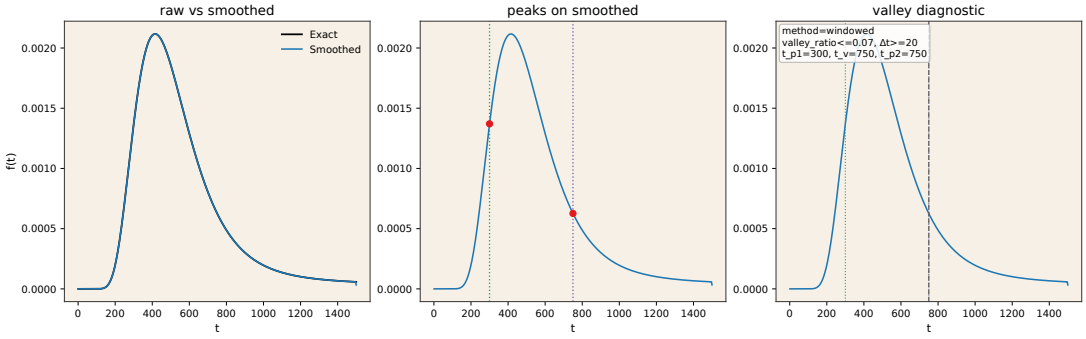


Figure 9: R1: bimodality diagnostic (smoothing and peak detection).

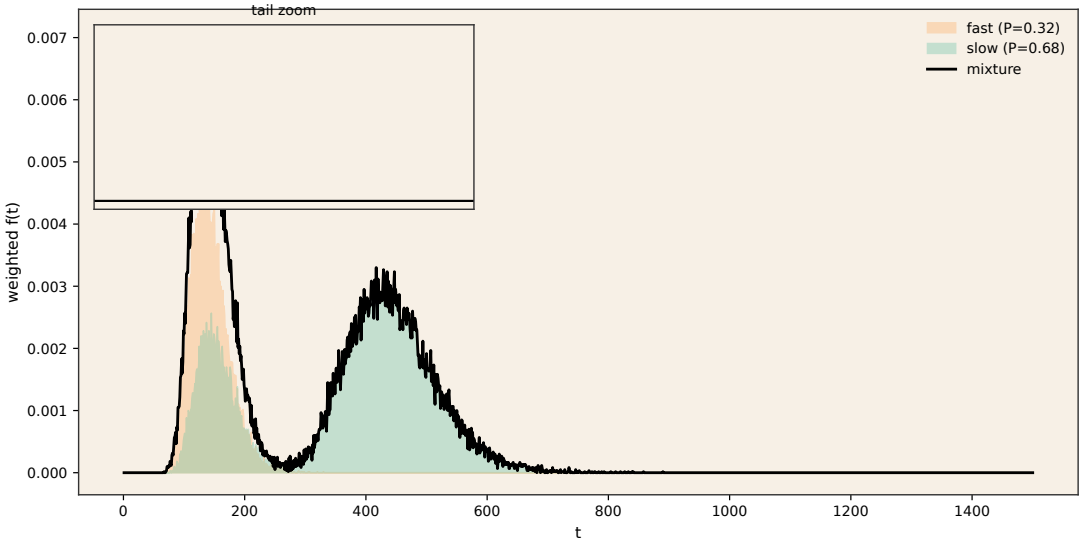


Figure 10: R1: channel decomposition and mixture.

6.2 R7: semipermeable pore shortcut vs long detour

R7 inserts a single semipermeable door on the main corridor and a U-shaped detour, mimicking a pore shortcut competing with a longer bypass.

Configuration Card $N = 60$, $q = 0.8$, $g = (-0.20, 0)$ with reflecting boundaries; start=(10,30), target=(50,30). The reachable set is the main corridor $y = 30$, $x = 10..50$ plus a short U-shaped detour (left column $x = 29$, $y = 1..30$, top edge $y = 1$, $x = 29..31$, right column $x = 31$, $y = 1..30$), with reflecting walls elsewhere. A semipermeable door sits at $(30, 30) \leftrightarrow (31, 30)$ with $p_{\text{pass}} = 0.8$, and local bias is applied only along the corridor/branch (main corridor right, left column up, top edge right, right column down) with $\delta = 0.95$. The channel rule marks any visit to the detour (upper segments of $x = 29$ or $x = 31$, or the top edge $y = 1$) as slow; otherwise the path stays on $y = 30$ and is fast. Metrics: $t_{p1} = 140$, $t_v = 280$, $t_{p2} = 428$; peak ratio= 0.294; valley ratio= 0.066; $P_{\text{fast}} = 0.248$.

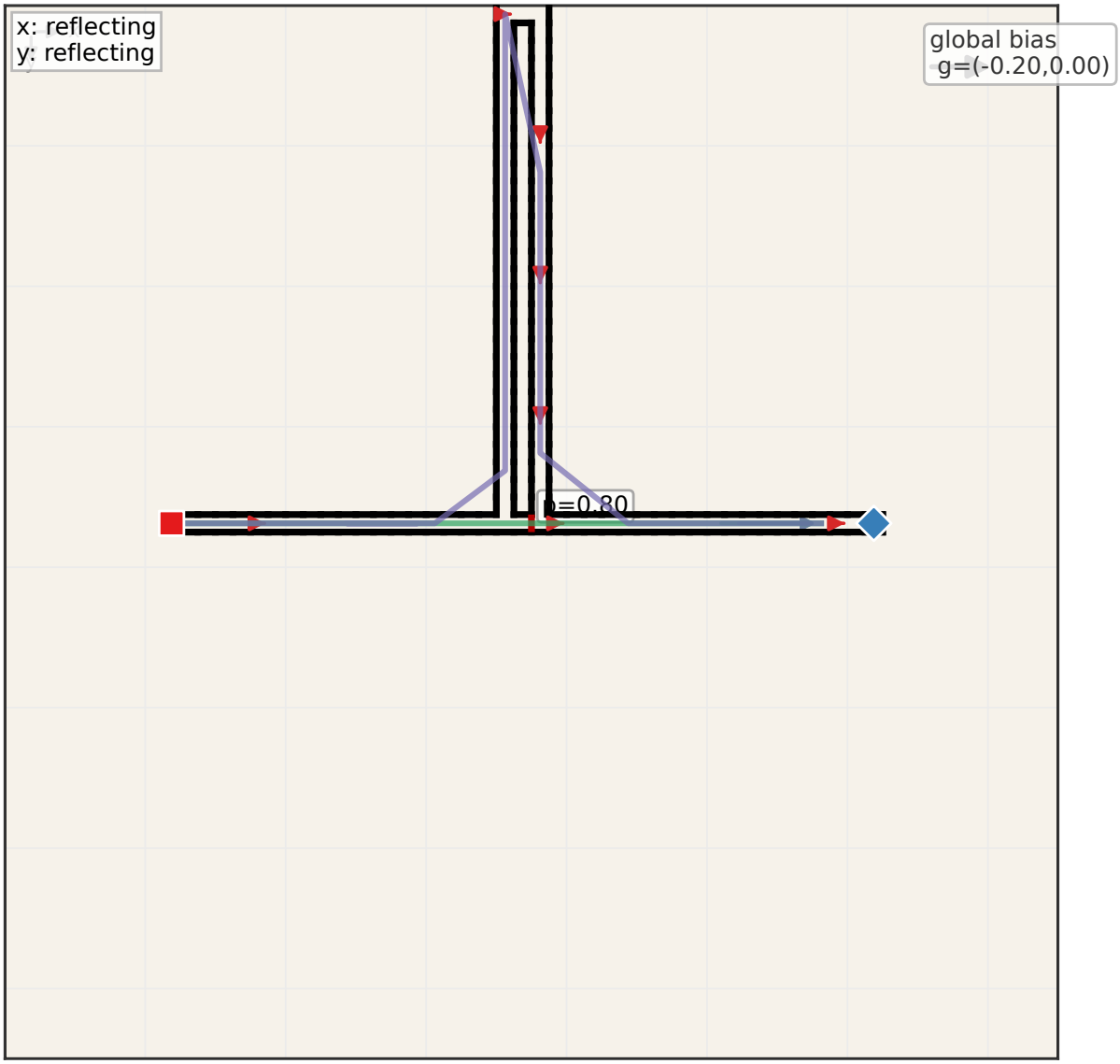


Figure 11: R7: environment schematic.

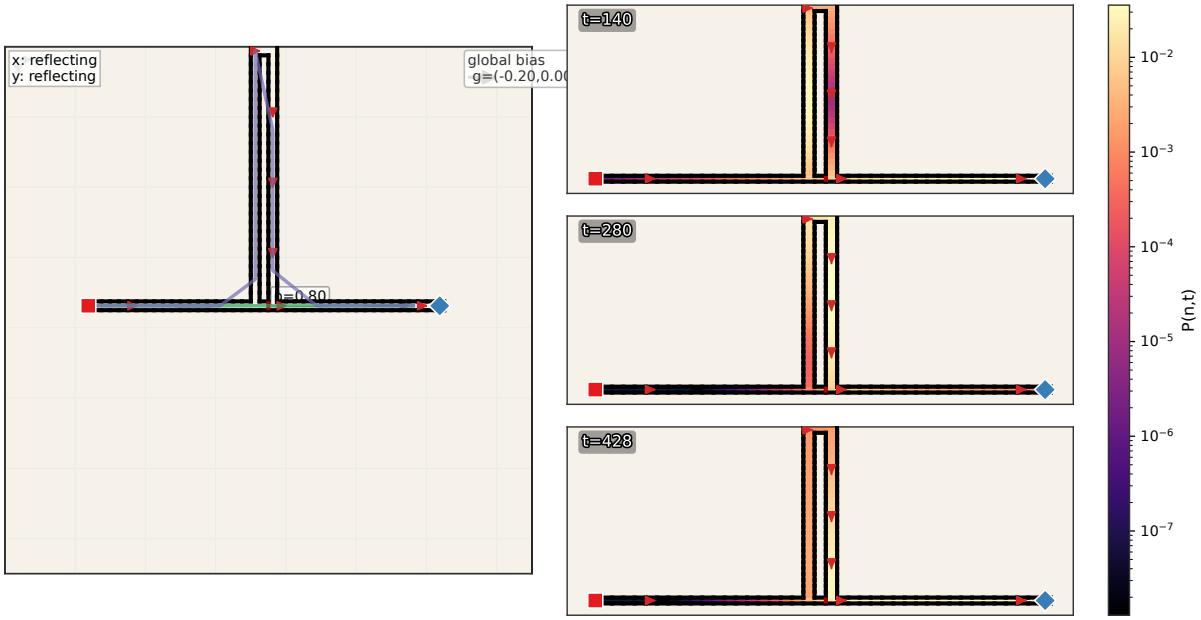


Figure 12: R7: environment and $P(n,t)$ slices at t_{p1}, t_v, t_{p2}.

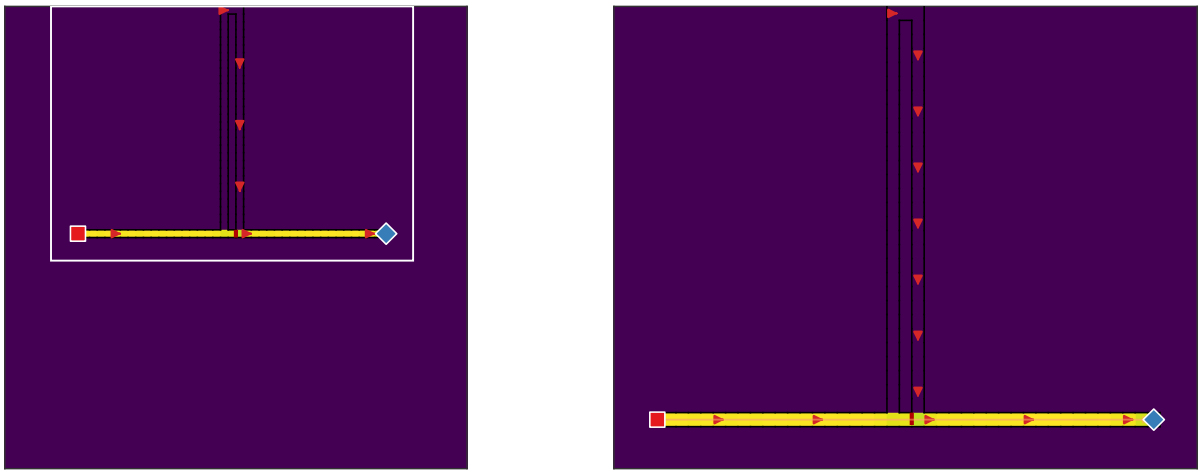


Figure 13: R7: fast-channel path density with representative paths (full + ROI).

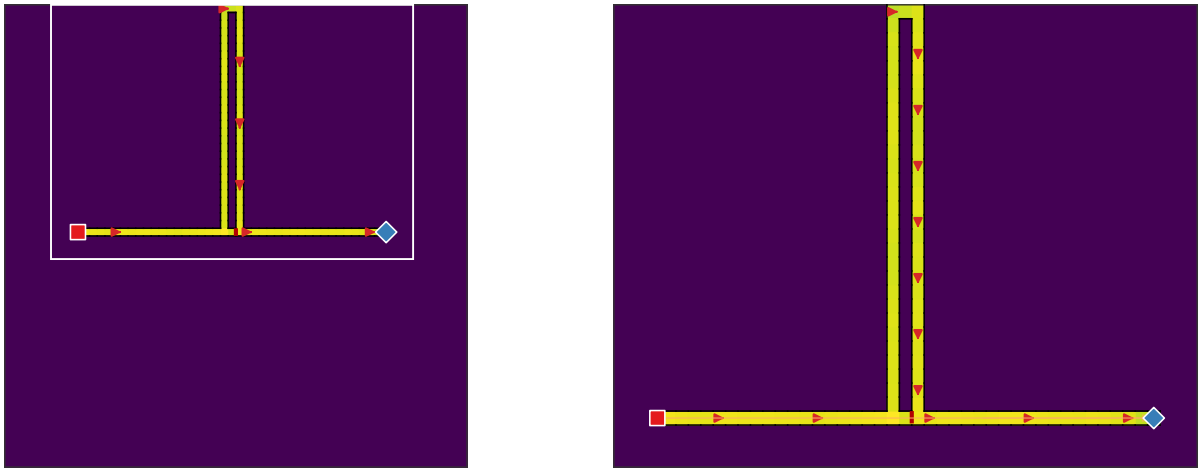


Figure 14: R7: slow-channel path density with representative paths (full + ROI).

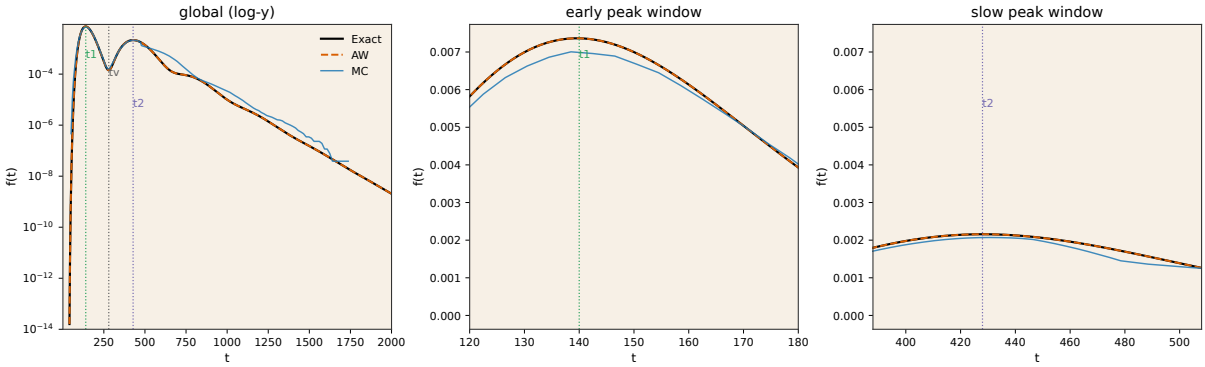


Figure 15: R7: multiscale FPT plot (Exact/AW/MC overlay).

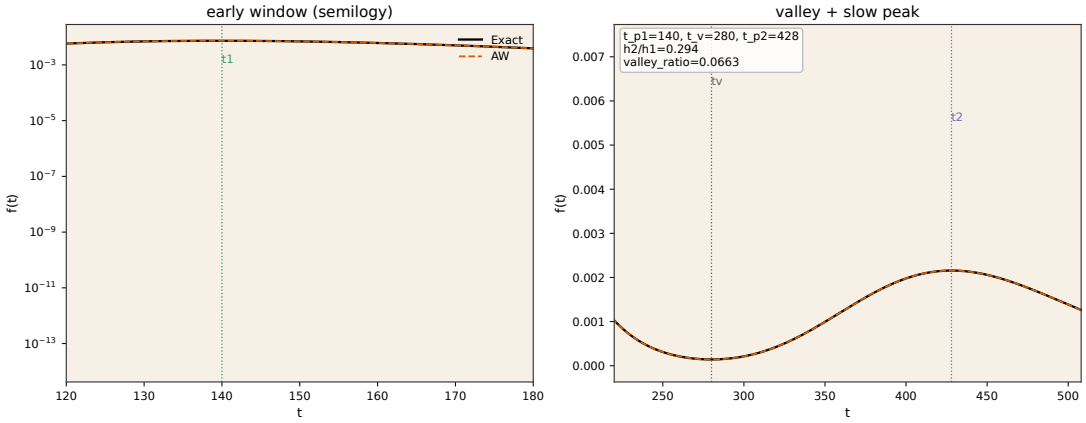


Figure 16: R7: peak–valley zoom.

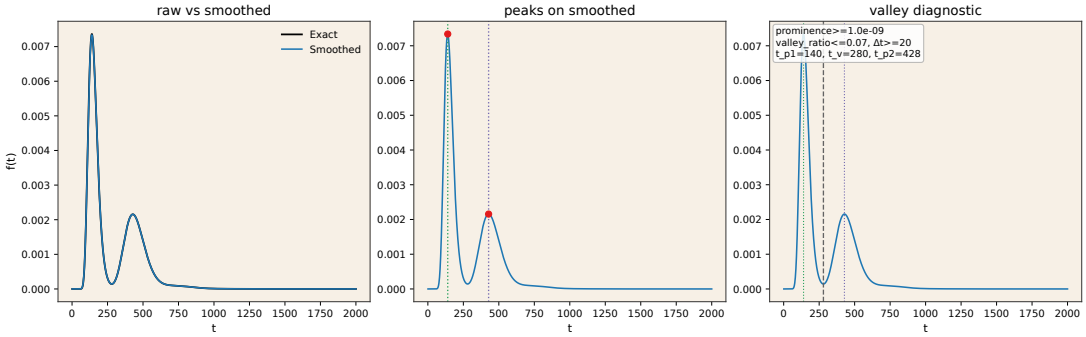


Figure 17: R7: bimodality diagnostics.

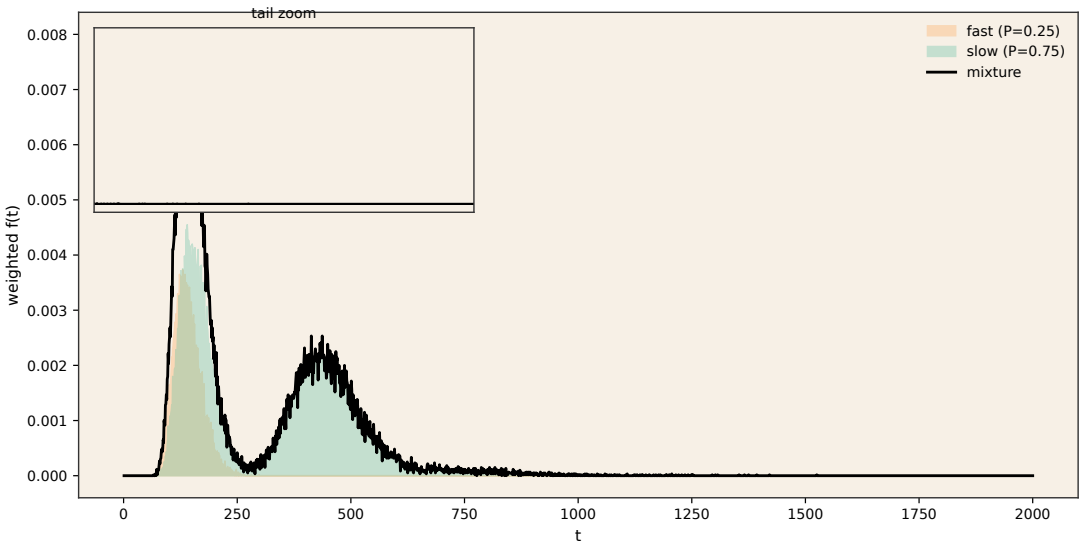


Figure 18: R7: channel decomposition and mixture.

6.3 C3: local active track vs long detour loop

C3 introduces a strong local-bias transport track (fast channel) and a long detour loop (slow channel), mimicking an internal active-transport lane with a bypass.

Configuration Card $N = 60$, $q = 0.8$, $g = (-0.15, 0)$ with reflecting boundaries; start=(10,30), target=(50,30). The reachable set is a fast track $y = 29$, $x = 10..50$ plus a slow loop (left column $x = 10$, $y = 30..60$, bottom edge $y = 60$, $x = 10..50$, right column $x = 50$, $y = 30..60$), connected to start/target via $(10, 30) \leftrightarrow (10, 29)$ and $(50, 29) \leftrightarrow (50, 30)$. Local bias drives the track rightward with $\delta = 0.95$; the detour follows down/right/up with $\delta = 0.55$; and the entry point $(10, 30)$ adds a weak downward arrow $\delta = 0.35$. The channel rule marks any visit to the detour set ($x = 10, y \geq 30$ or $x = 50, y \geq 30$ or $y = 60$) as slow; otherwise the path reaches the target along $y = 29$ and is fast. Metrics: $t_{p1} = 160$, $t_v = 388$, $t_{p2} = 702$; peak ratio= 0.231; valley ratio= 0.022; $P_{\text{fast}} = 0.293$.

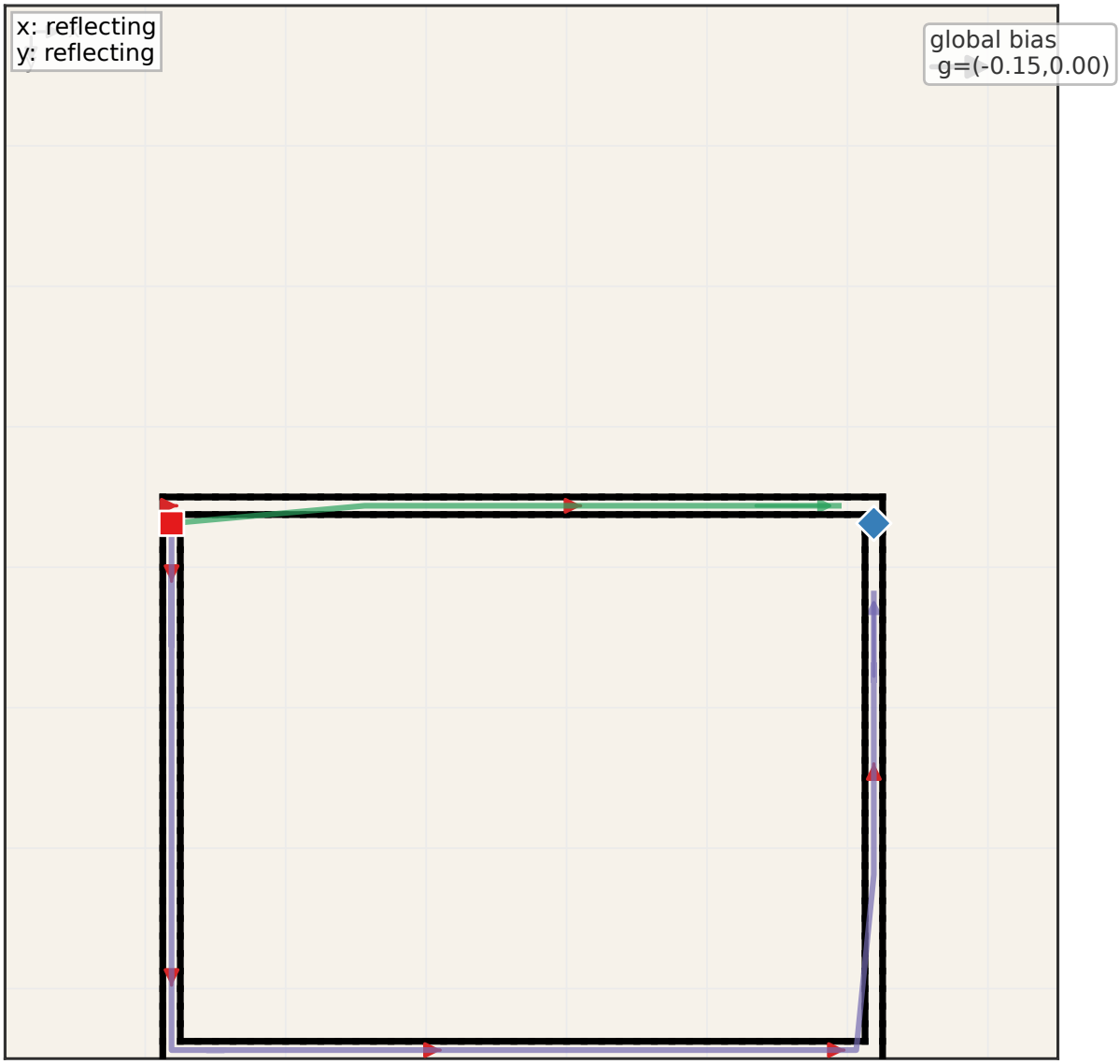


Figure 19: C3: environment schematic.

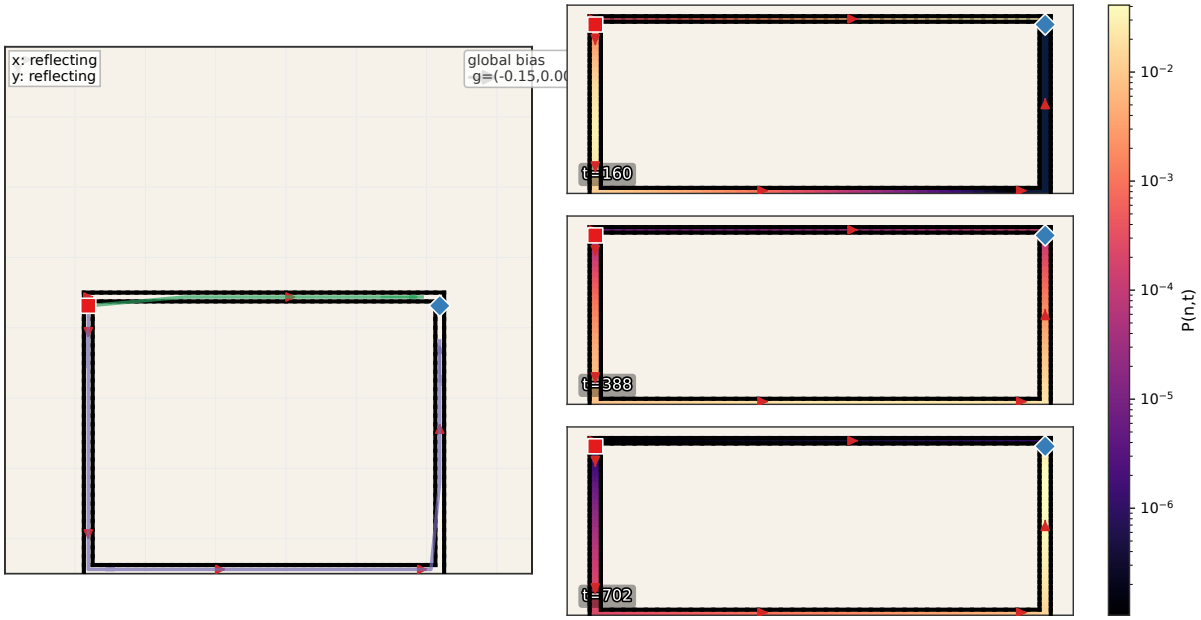


Figure 20: C3: environment and $P(n,t)$ slices at t_{p1}, t_v, t_{p2}.

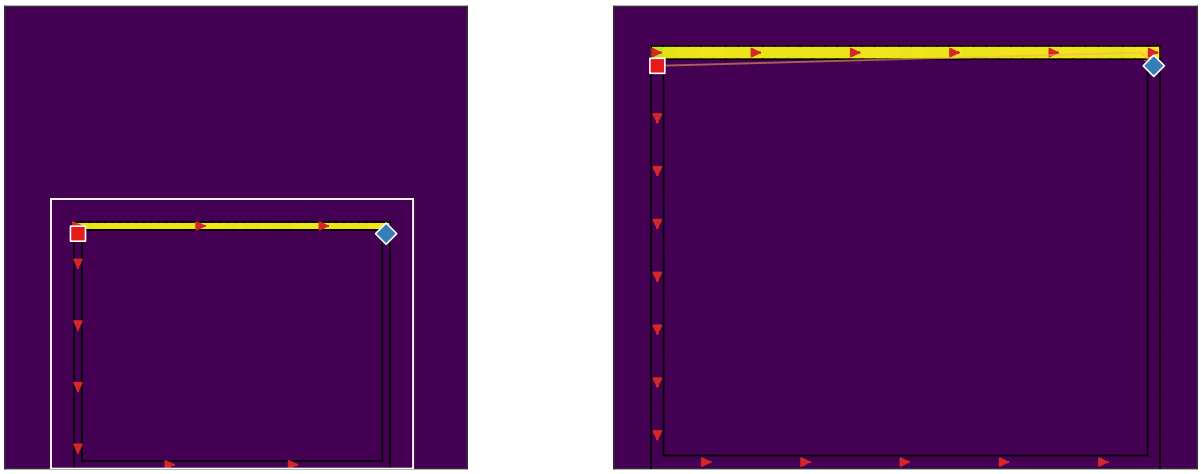


Figure 21: C3: fast-channel path density with representative paths (full + ROI).

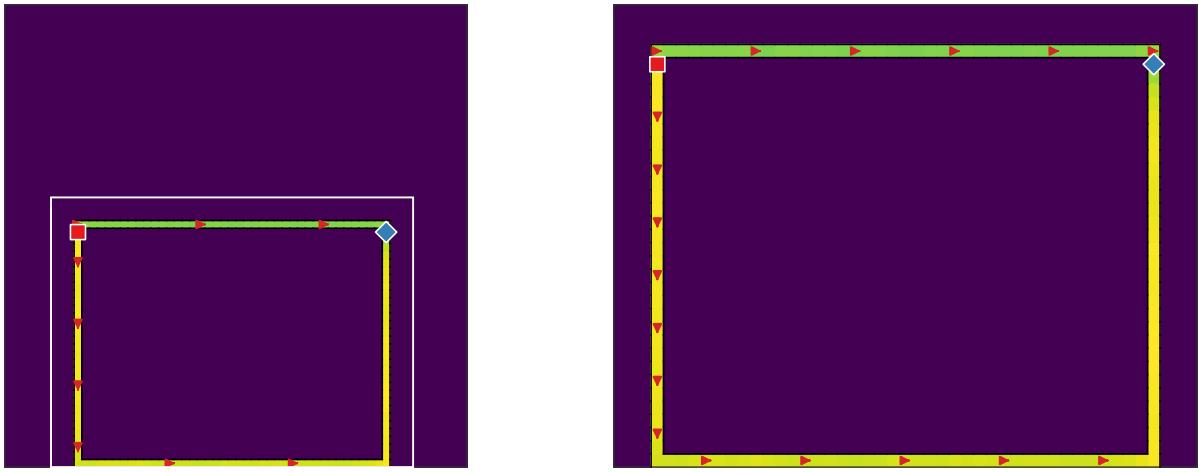


Figure 22: C3: slow-channel path density with representative paths (full + ROI).

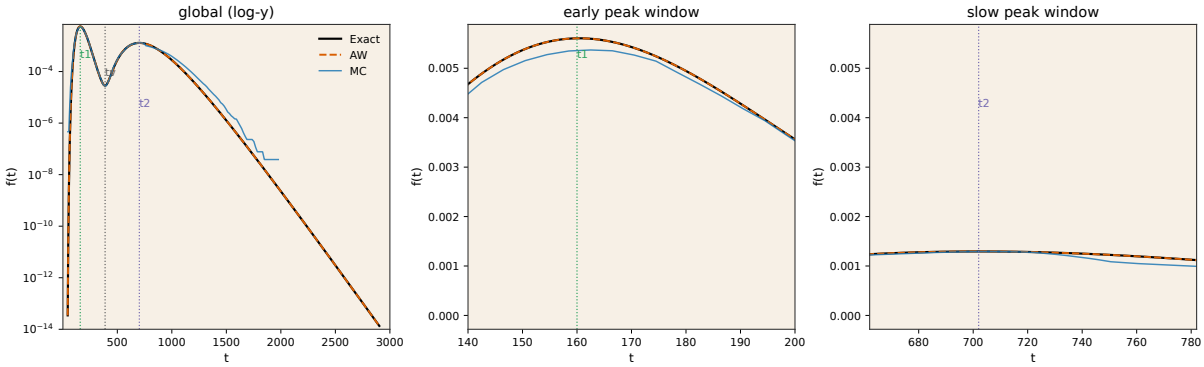


Figure 23: C3: multiscale FPT plot (Exact/AW/MC overlay).

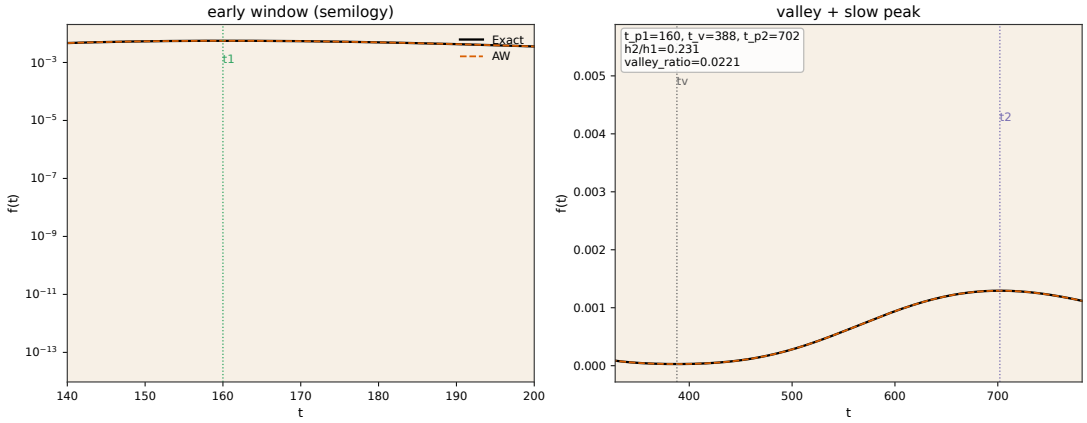


Figure 24: C3: peak–valley zoom.

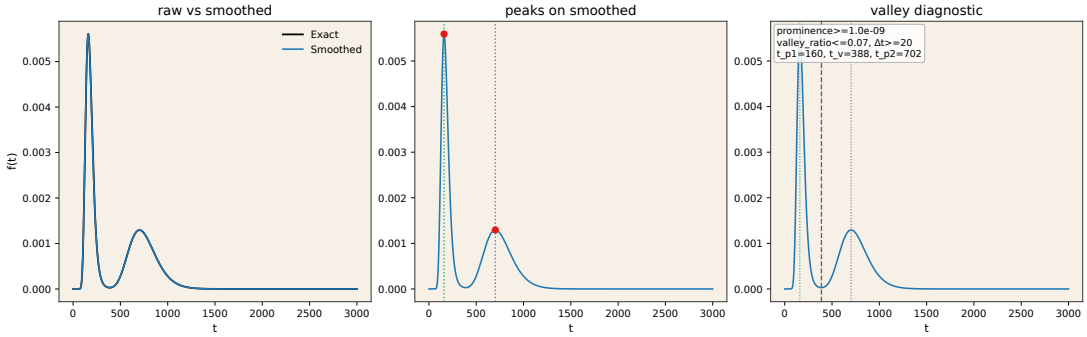


Figure 25: C3: bimodality diagnostics.

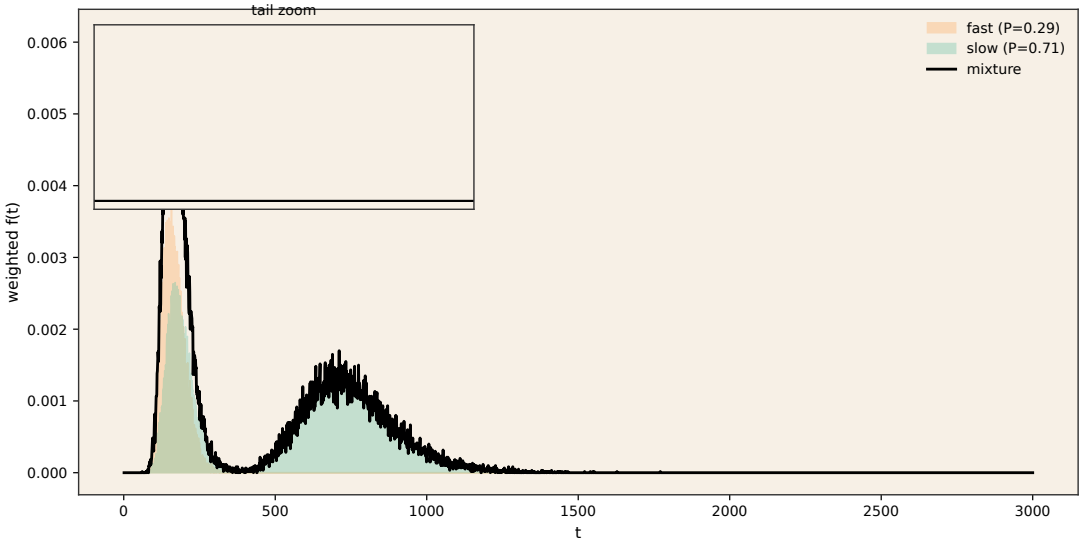


Figure 26: C3: channel decomposition and mixture.

6.4 R6: parallel lanes with a door array slowdown

R6 uses two nearly equal-length lanes; the slow channel arises from the door array.

Configuration Card $N = 60,\ q = 0.8,\ g = (0, 0)$ with reflecting boundaries; start=(10,30), target=(50,30). The reachable set is a rectangular loop with horizontal lanes $y = 20$ and $y = 40$ for $x = 10..50$, connected by vertical sides $x = 10, 50$ for $y = 20..40$, and start/target at the midpoints of the left/right sides. Each horizontal edge on the slow lane $(x, 40) \leftrightarrow (x + 1, 40)$ is a door with $p_{\text{pass}} = 0.1$, and local bias follows the lanes (right, $\delta = 0.95$) with softer turning bias on the vertical sides ($\delta = 0.6$). The channel rule marks any visit to the $y = 40$ lane as slow; otherwise the path reaches the target via the $y = 20$ lane and is fast. Metrics: $t_{p1} = 347,\ t_v = 1021,\ t_{p2} = 2160$; peak ratio= 0.141; valley ratio= 0.063; $P_{\text{fast}} = 0.498$.

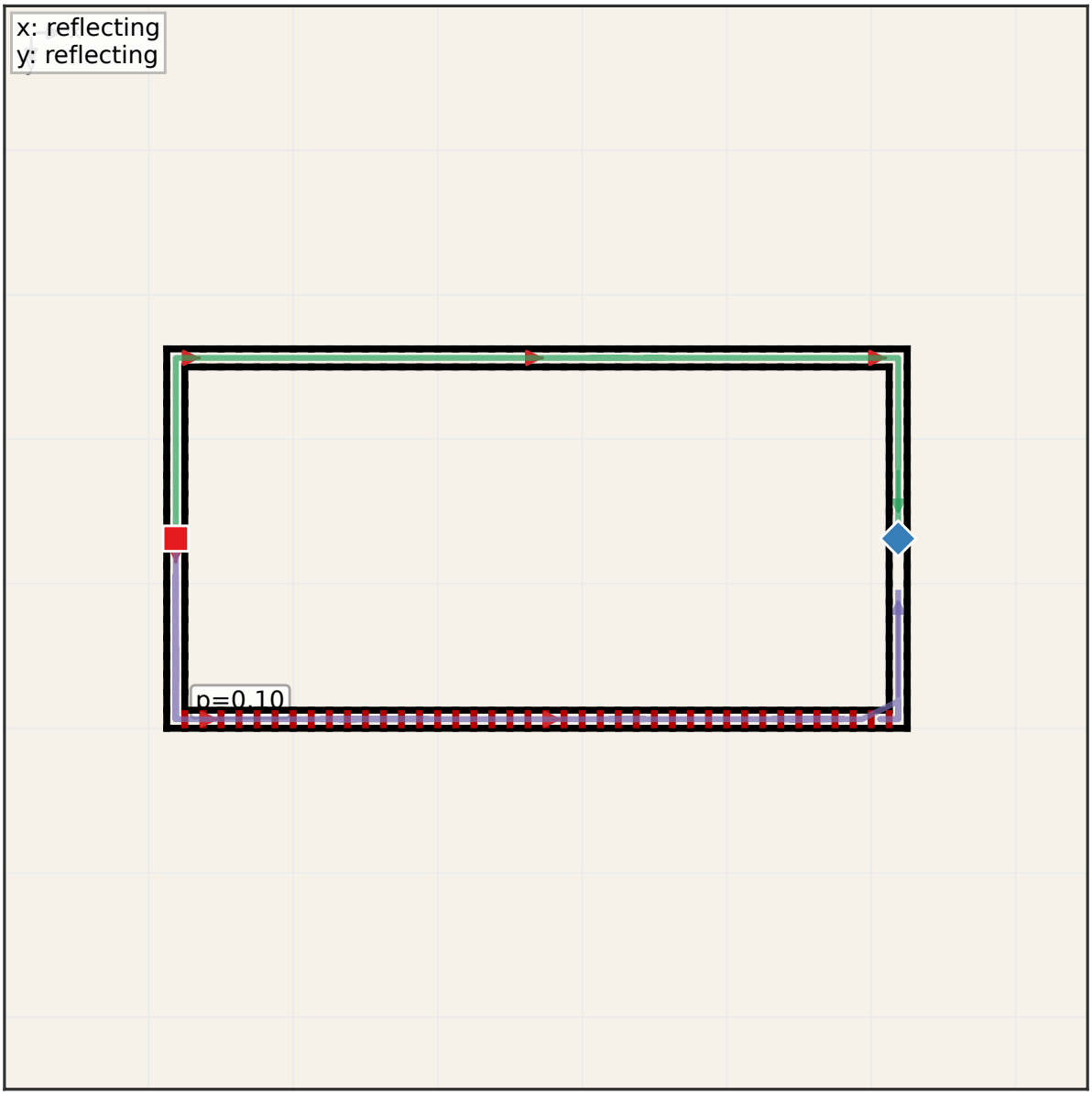


Figure 27: R6: environment schematic.

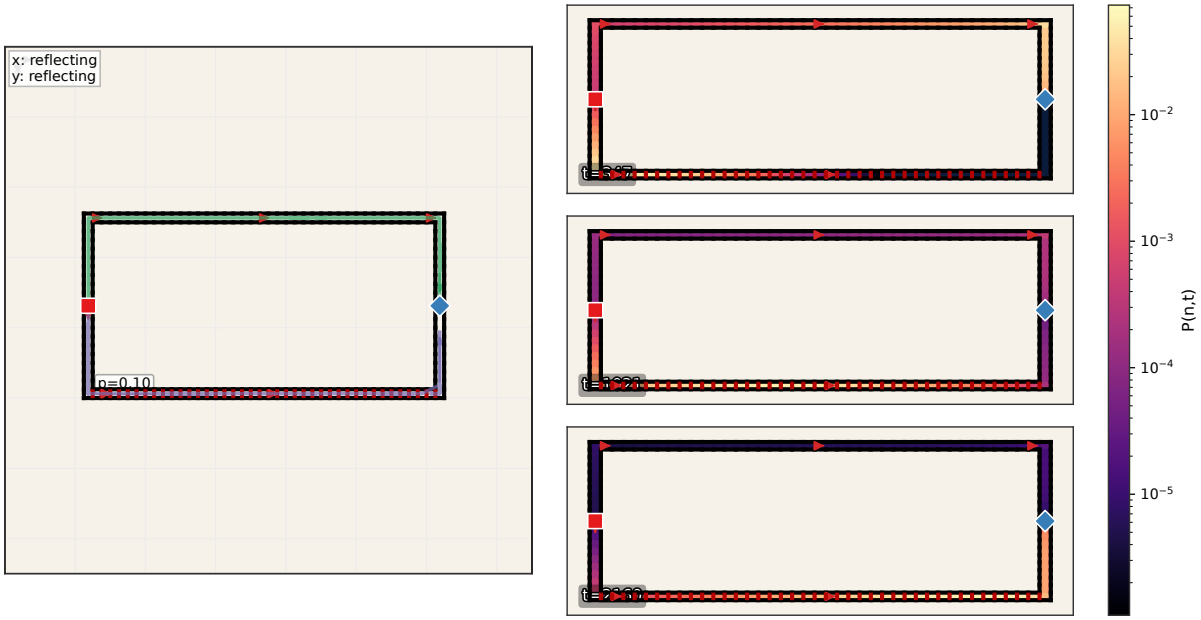


Figure 28: R6: environment and $P(n,t)$ slices at t_{p1}, t_v, t_{p2}.

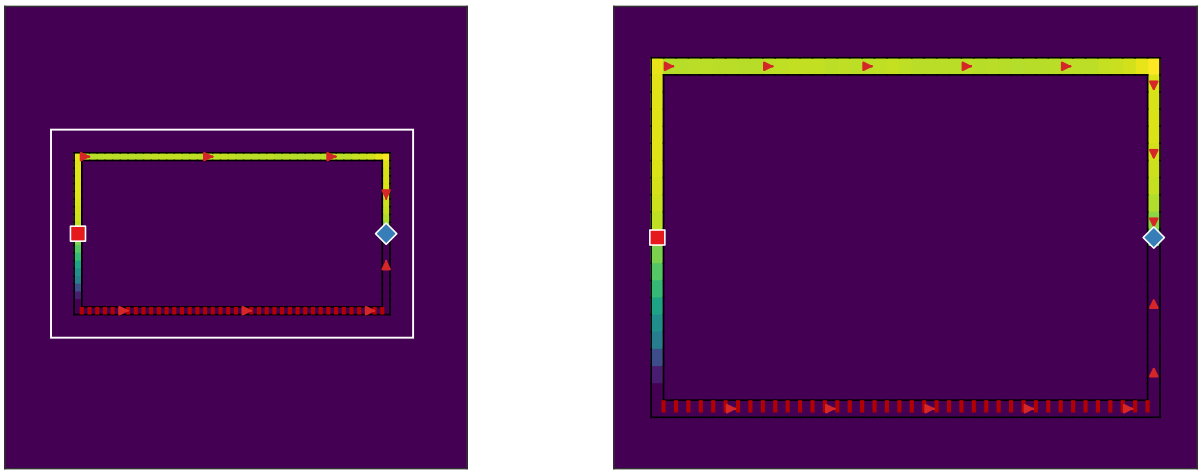


Figure 29: R6: fast-channel path density + representative paths (full + ROI).

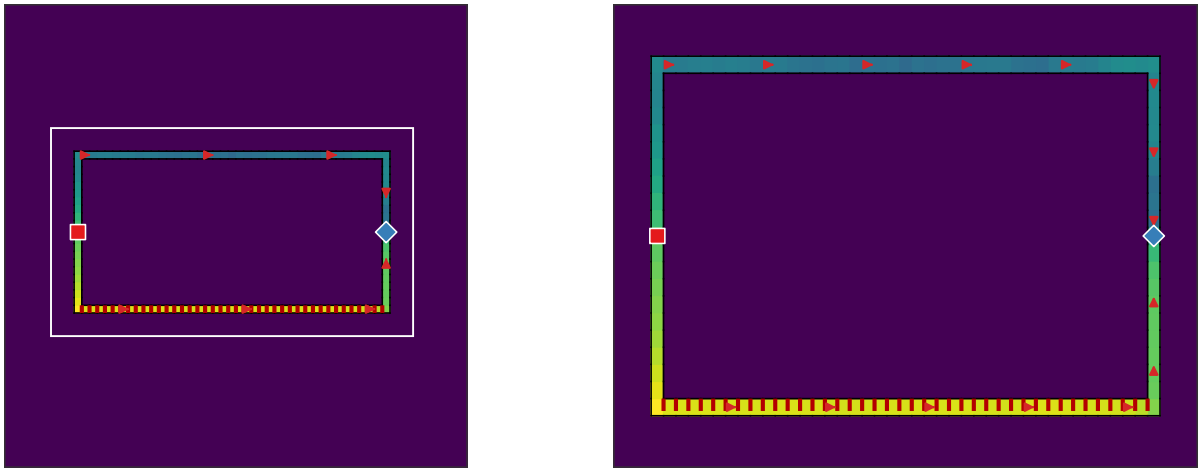


Figure 30: R6: slow-channel path density + representative paths (full + ROI).

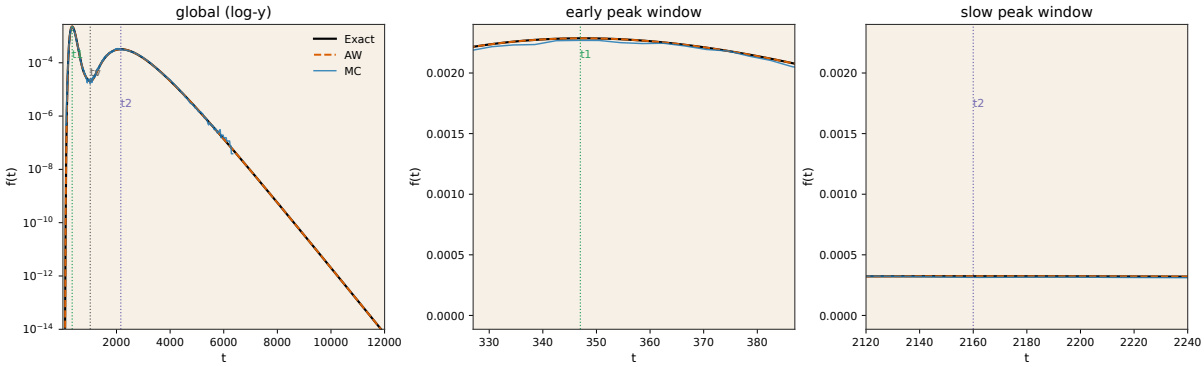


Figure 31: R6: multiscale FPT plot (Exact/AW/MC overlay).

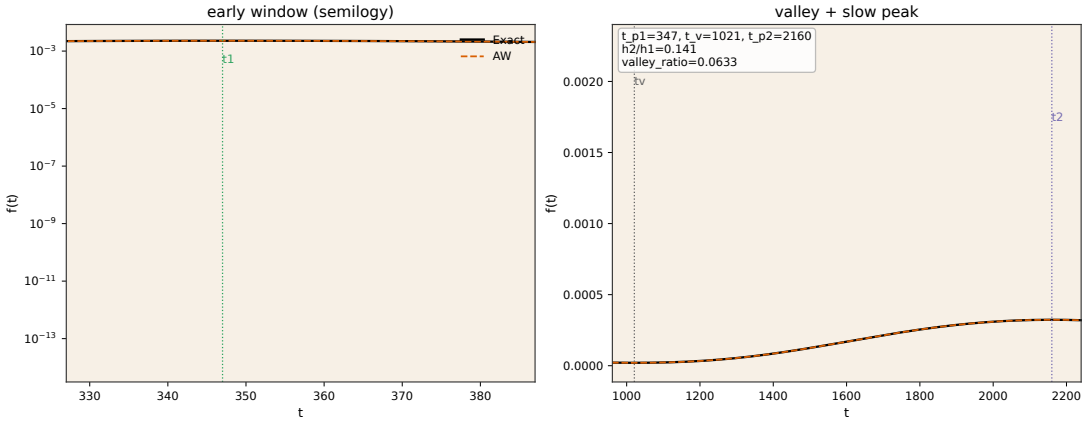


Figure 32: R6: peak–valley zoom.

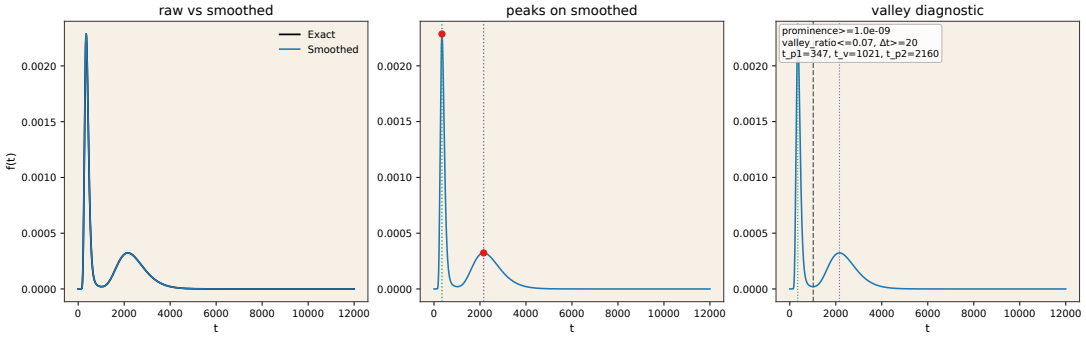


Figure 33: R6: bimodality diagnostic.

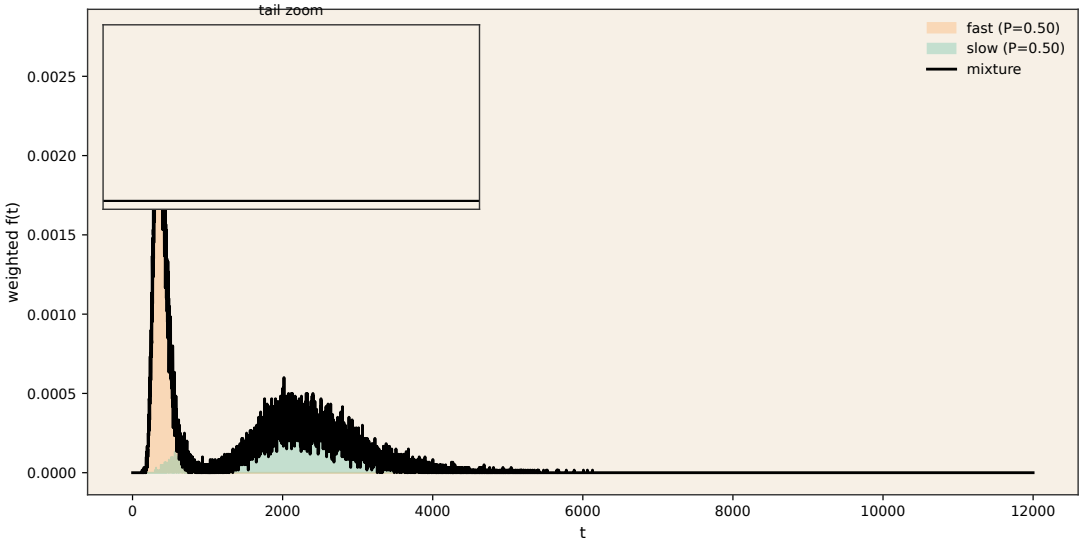


Figure 34: R6: channel decomposition and mixture.

6.5 NB4: perimeter clockwise belt (no internal barrier/door)

NB4 modifies only the outer boundary: sticky sites plus a clockwise local bias. The target is two steps counterflow from the start, yielding a short counterflow path vs a long clockwise loop.

Configuration Card $N = 60$,
; $q = 0.8$,
; $g = (0.00, 0.00)$ with reflecting boundaries; start=(12,60), target=(10,60). The full domain is accessible and there are no internal barriers/doors; only the perimeter is sticky with factor 0.2 (all $y = 1, 60$ and all $x = 1, 60$). A clockwise local bias runs along the boundary (bottom R, right U, top L, left D) with $\delta = 0.63$, including corners. The channel rule marks any hit of the top edge $y = 1$ before absorption as slow; otherwise the short counterclockwise hop along the bottom edge is fast. Metrics: $t_{p1} = 6$,
; $t_v = 389$,
; $t_{p2} = 642$; peak ratio= 0.932; valley ratio= 0.062; $P_{textfast} = 0.104$.



Figure 35: NB4: environment schematic.

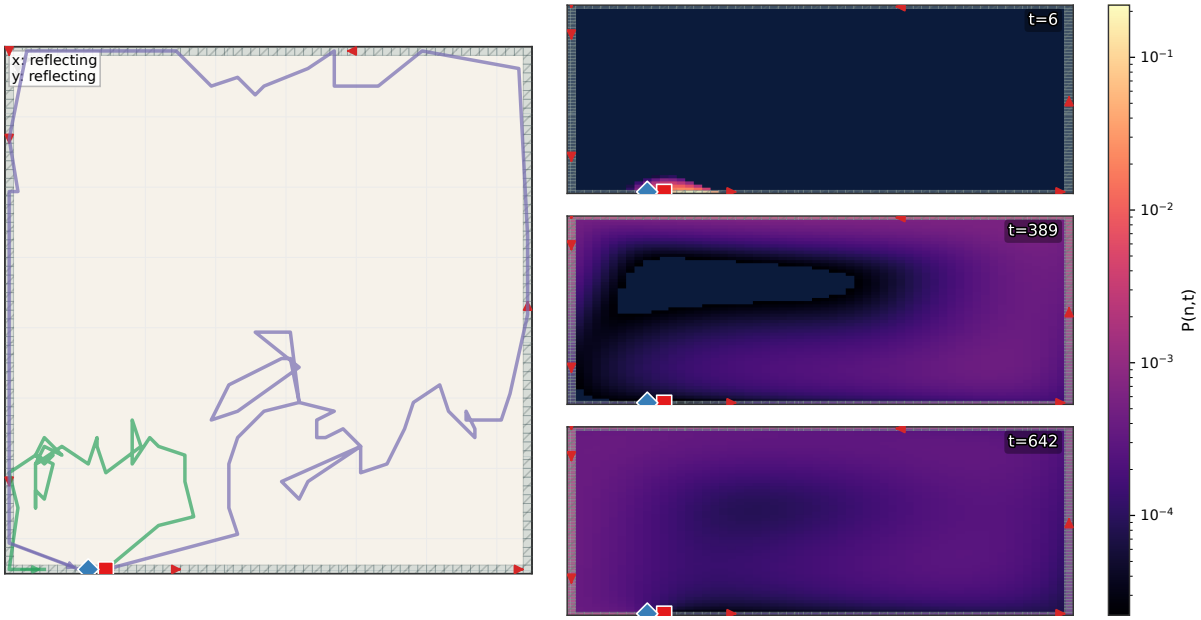


Figure 36: NB4: environment and $P(n,t)$ slices at t_{p1}, t_v, t_{p2}.

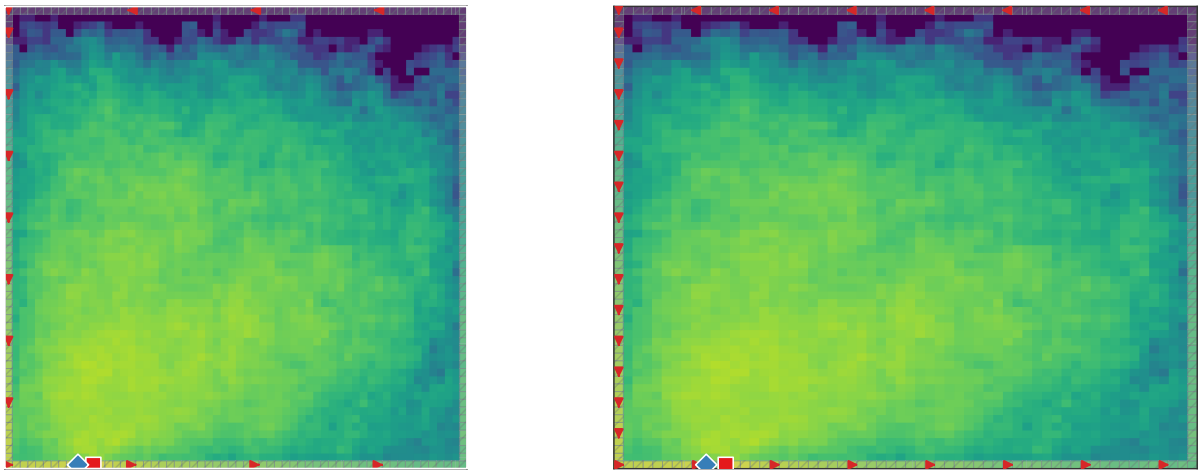


Figure 37: NB4: fast-channel path density + representative paths (full + ROI).

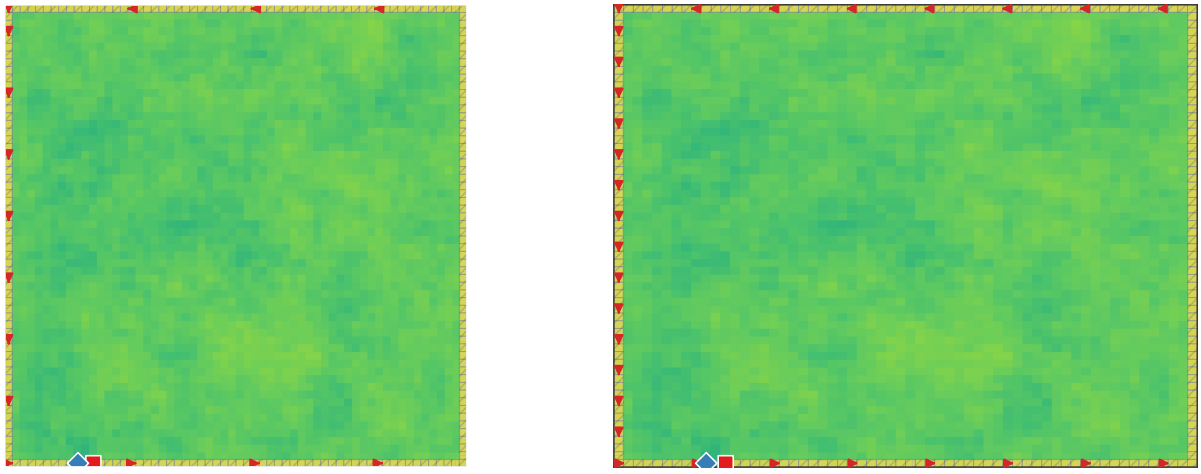


Figure 38: NB4: slow-channel path density + representative paths (full + ROI).

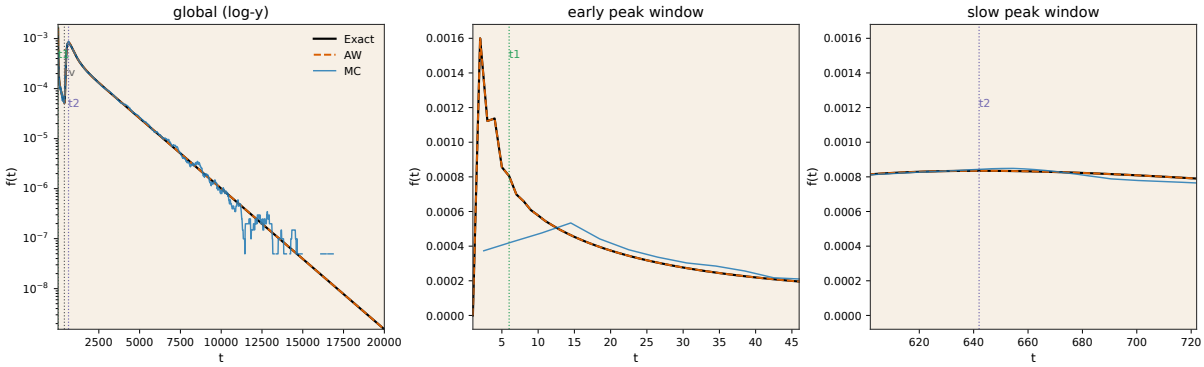


Figure 39: NB4: multiscale FPT plot (Exact/AW/MC overlay).

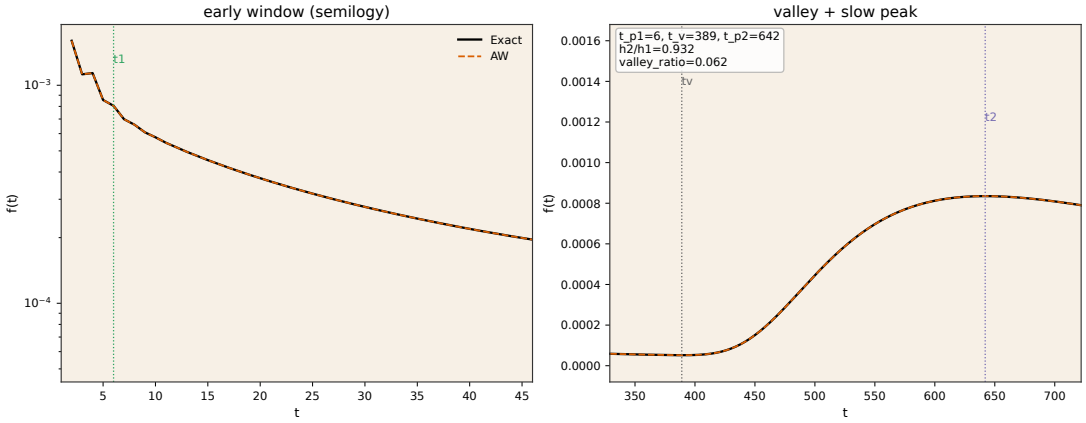


Figure 40: NB4: peak–valley zoom.

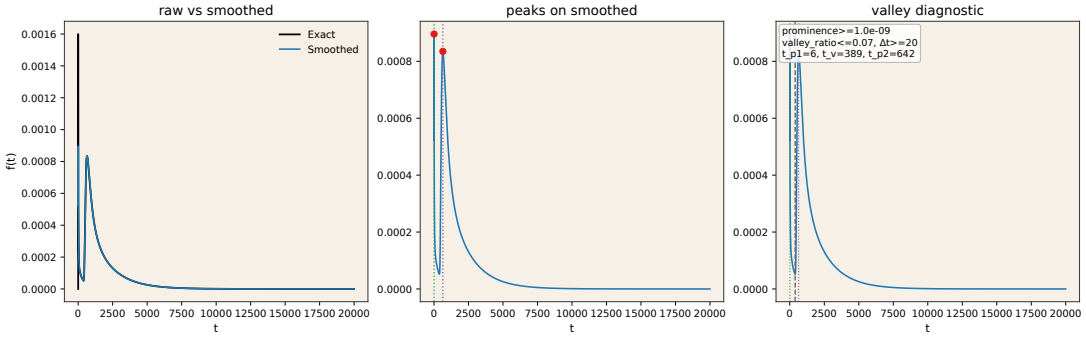


Figure 41: NB4: bimodality diagnostic.

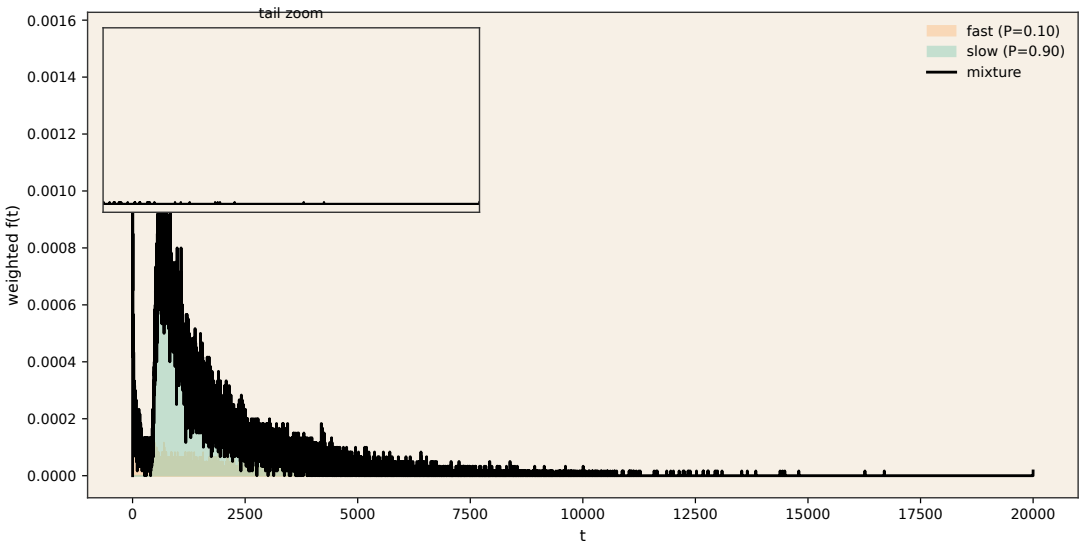


Figure 42: NB4: channel decomposition and mixture.

6.6 NB5: perimeter belt + global bias

NB5 adds a global rightward drift ($g_x < 0$) on top of the NB4 boundary conveyor, strengthening the clockwise preference; fast paths still correspond to the short counterflow hop, while slow paths loop clockwise.

Configuration Card $N = 60$,
; $q = 0.8$,
; $g = (-0.10, 0.00)$ with reflecting boundaries; start=(12,60), target=(10,60). The full domain is accessible and there are no internal barriers/doors; only the perimeter is sticky with factor 0.2 (all $y = 1, 60$ and all $x = 1, 60$). A clockwise local bias runs along the boundary (bottom R, right U, top L, left D) with $\delta = 0.63$, and we add a global right bias $g_x = -0.10$. The channel rule marks any hit of the top edge $y = 1$ before absorption as slow; otherwise the short counterclockwise hop is fast. Metrics: $t_{p1} = 6$,
; $t_v = 379$,
; $t_{p2} = 621$; peak ratio= 0.930; valley ratio= 0.009; $P_{textfast} = 0.024$.

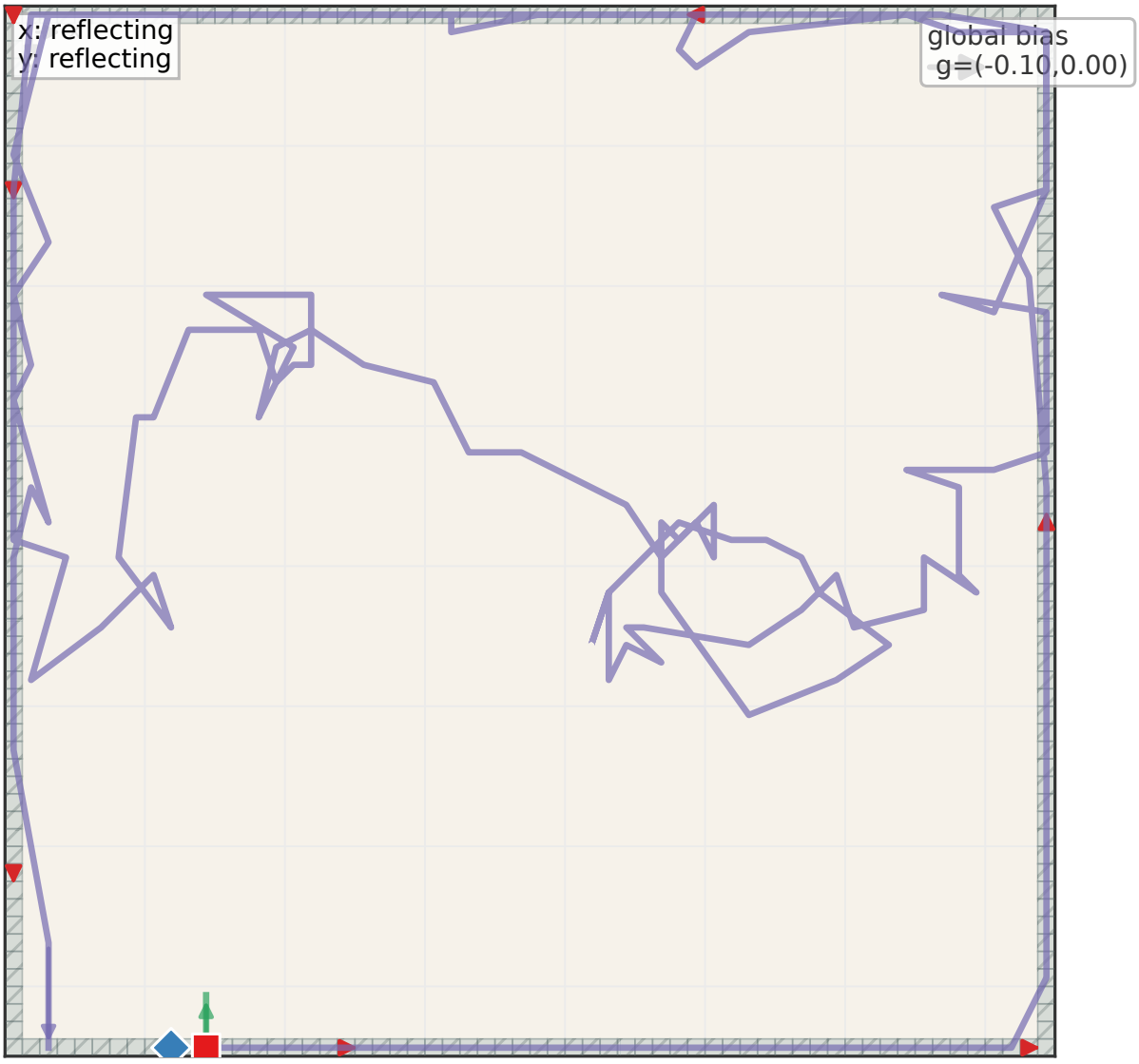


Figure 43: NB5: environment schematic.

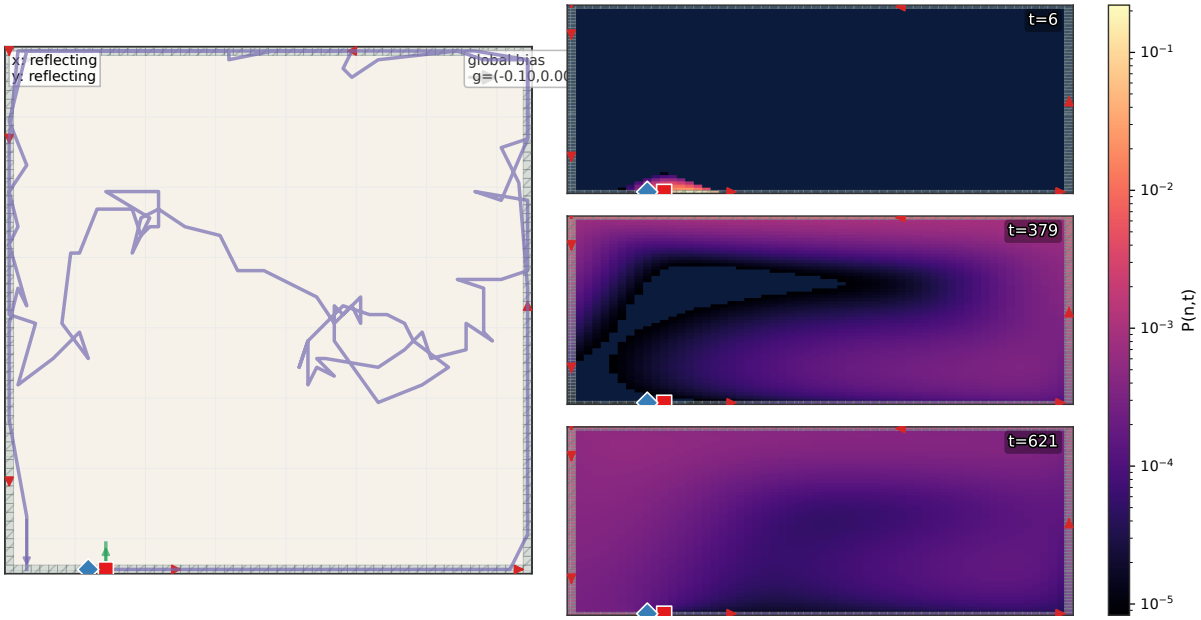


Figure 44: NB5: environment and $P(n,t)$ slices at t_{p1}, t_v, t_{p2}.

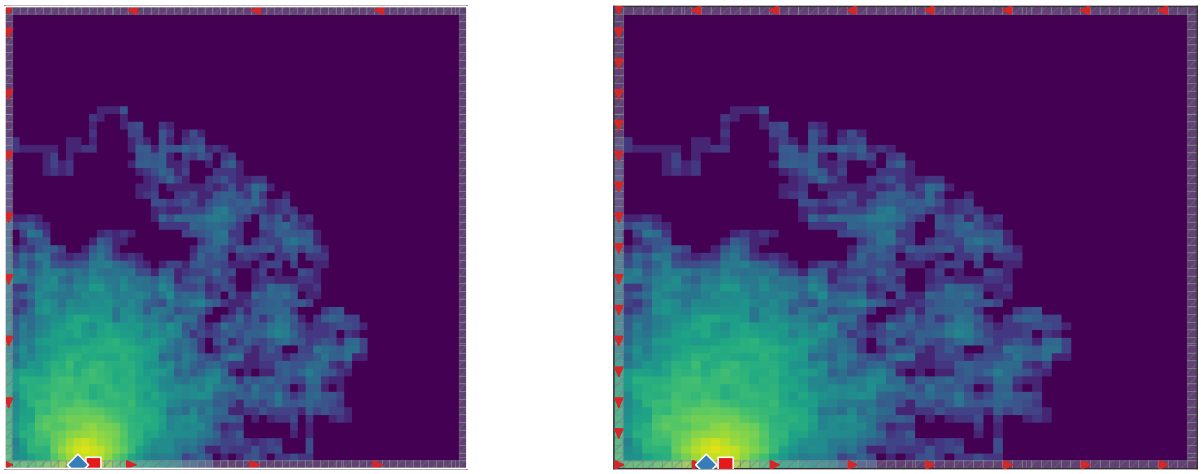


Figure 45: NB5: fast-channel path density + representative paths (full + ROI).

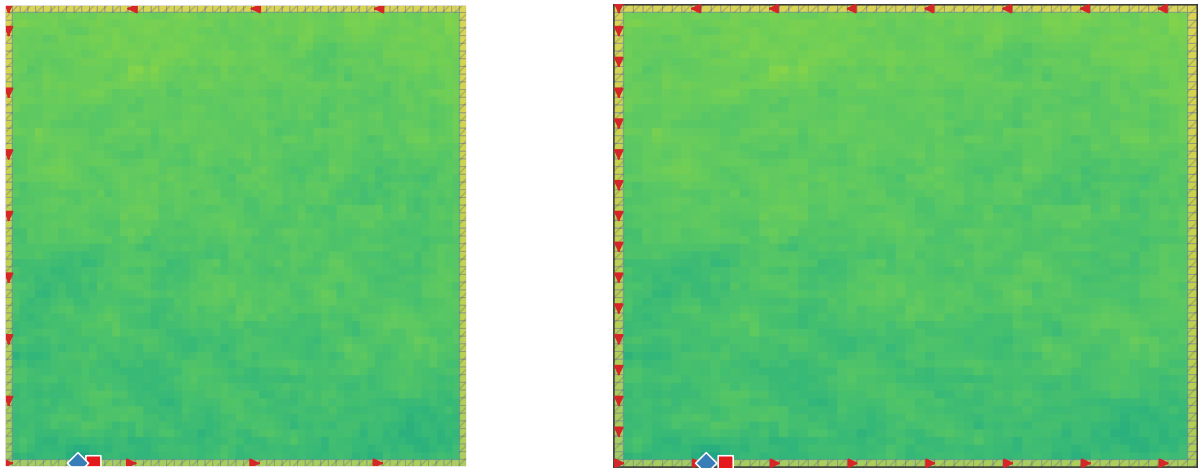


Figure 46: NB5: slow-channel path density + representative paths (full + ROI).

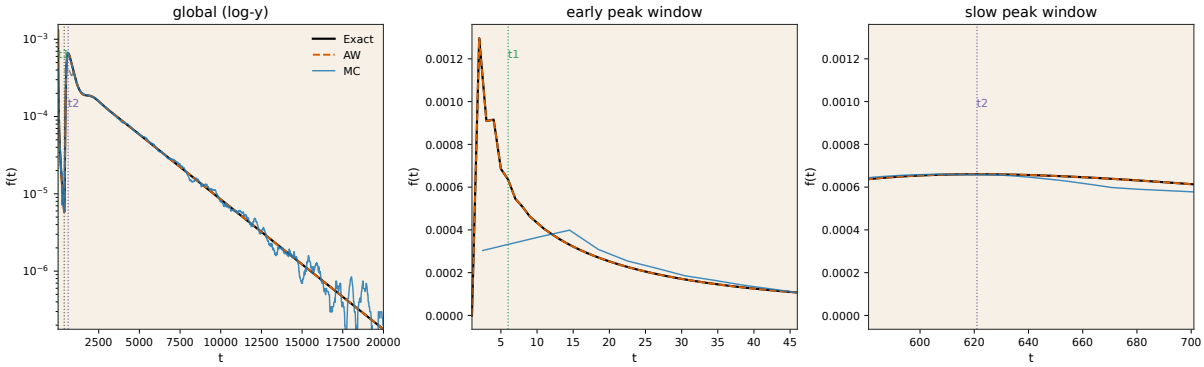


Figure 47: NB5: multiscale FPT plot (Exact/AW/MC overlay).

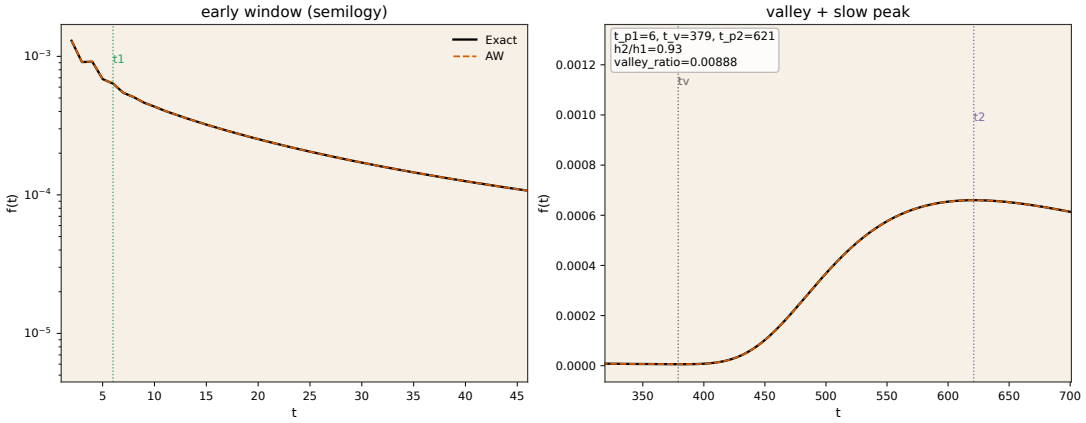


Figure 48: NB5: peak–valley zoom.

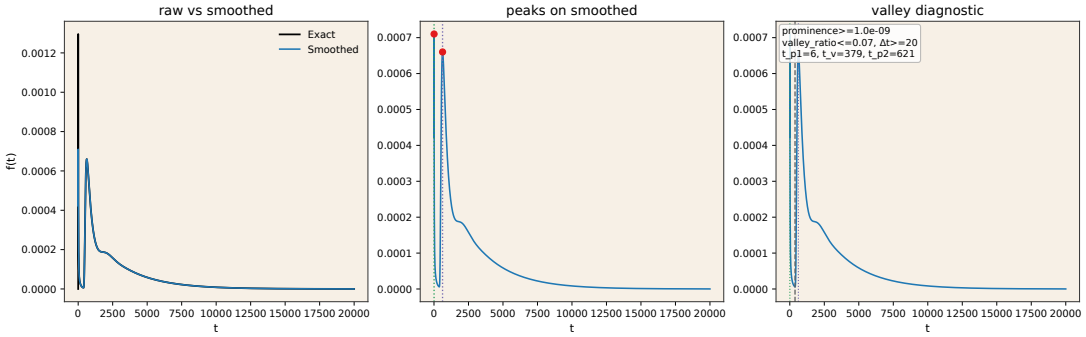


Figure 49: NB5: bimodality diagnostic.

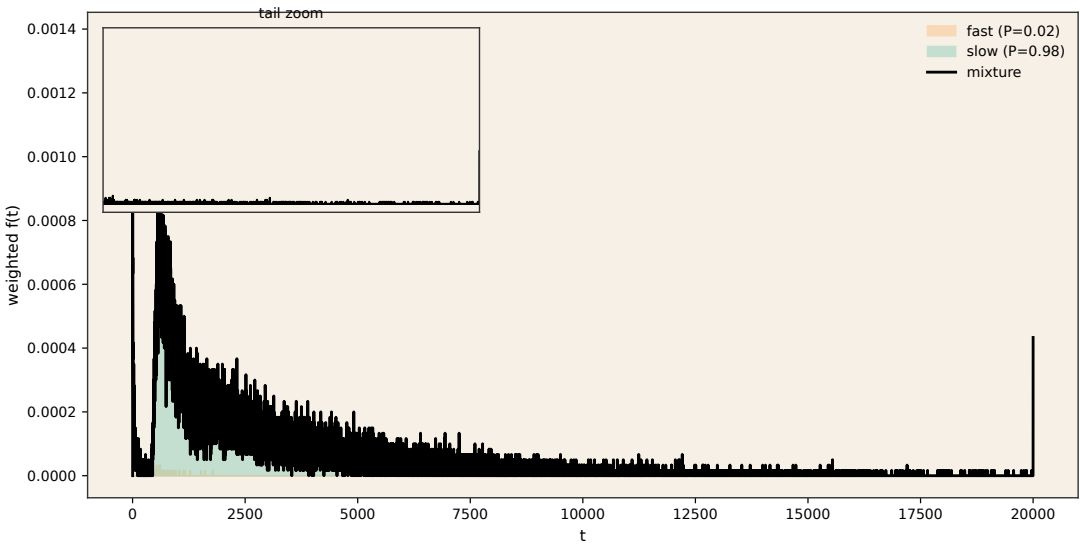


Figure 50: NB5: channel decomposition and mixture.

6.7 S1: soft two-track construction (turn at $y = 1$)

S1 removes all internal barriers/doors and uses sticky plus local arrows to create two "soft corridors": a short fast lane and a long detour along the top edge.

Configuration Card $N = 60,\ q = 0.8,\ g = (0, 0)$ with reflecting boundaries; start=(10,30), target=(50,30). The full domain is accessible and there are no internal barriers/doors. The fast lane is $y = 30,\ x = 11..49$ with sticky factor 0.05 and rightward bias $\delta = 0.95$. The slow lane follows the left column $x = 10,\ y = 2..30$ (up), the top edge $y = 1,\ x = 10..49$ (right), and the right column $x = 50,\ y = 1..29$ (down), with the same sticky factor 0.05 and weaker bias $\delta = 0.30$. The channel rule marks any hit of the top edge segment $y = 1$ before absorption as slow; otherwise it is fast. Metrics: $t_{p1} = 47,\ t_v = 240,\ t_{p2} = 363$; peak ratio= 0.641; valley ratio= 0.037; $P_{\text{fast}} = 0.127$.

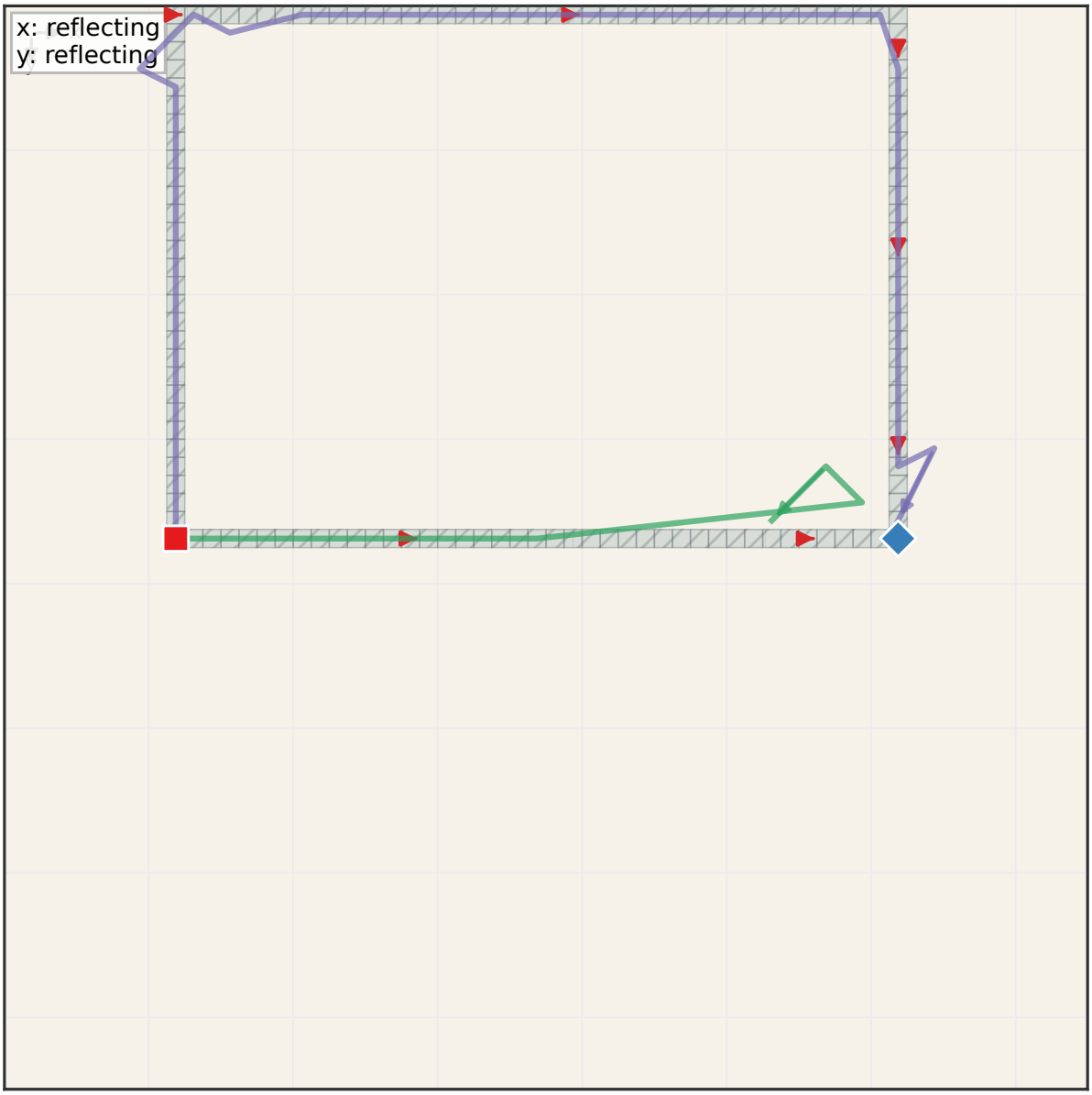


Figure 51: S1: environment schematic.

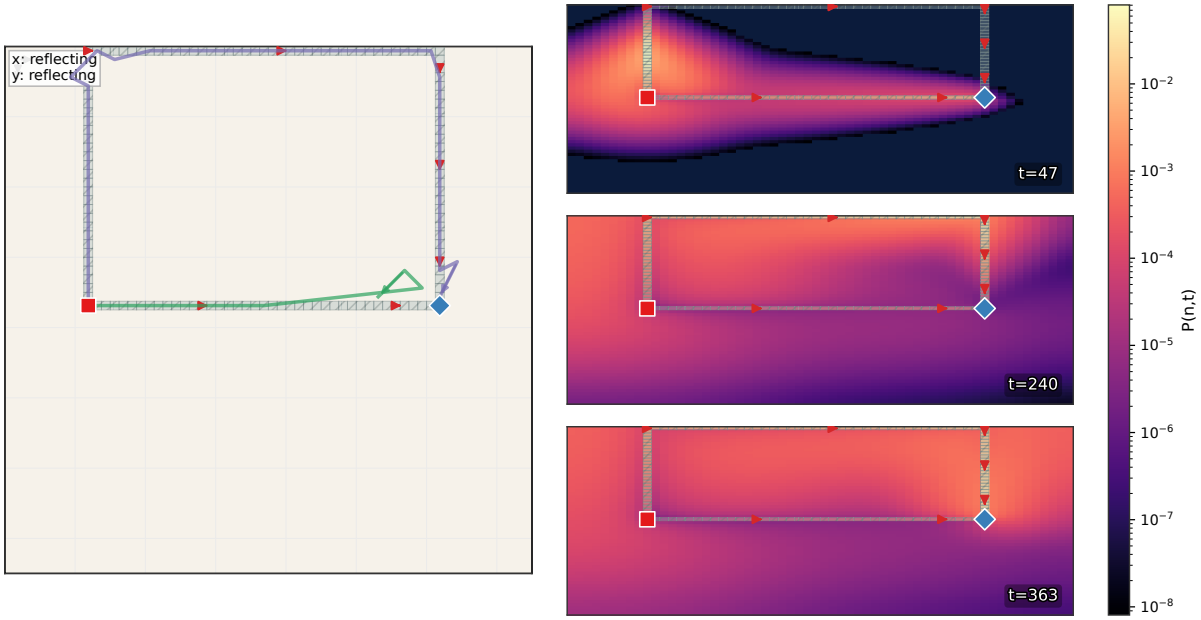


Figure 52: S1: environment and $P(n,t)$ slices at t_{p1}, t_v, t_{p2}.

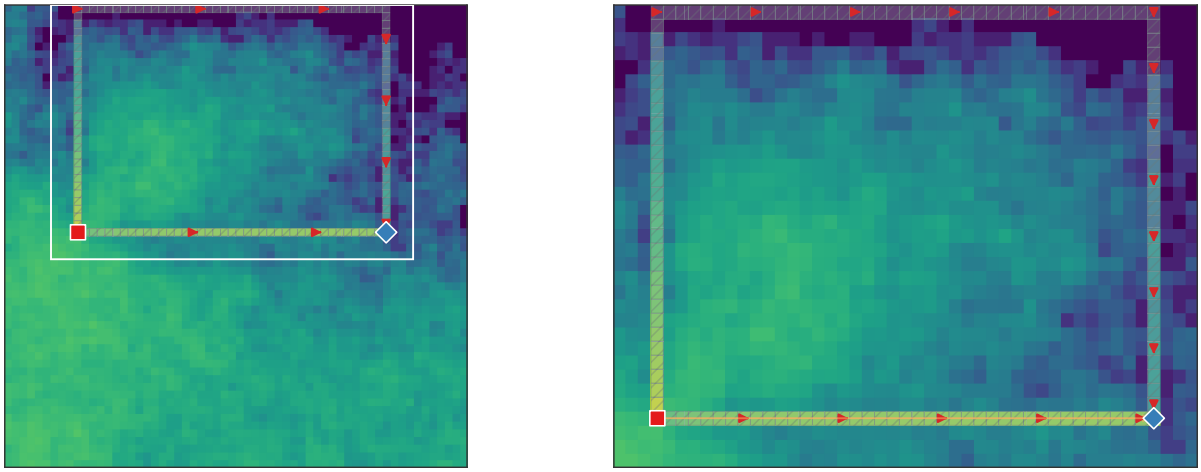


Figure 53: S1: fast-channel path density + representative paths (full + ROI).

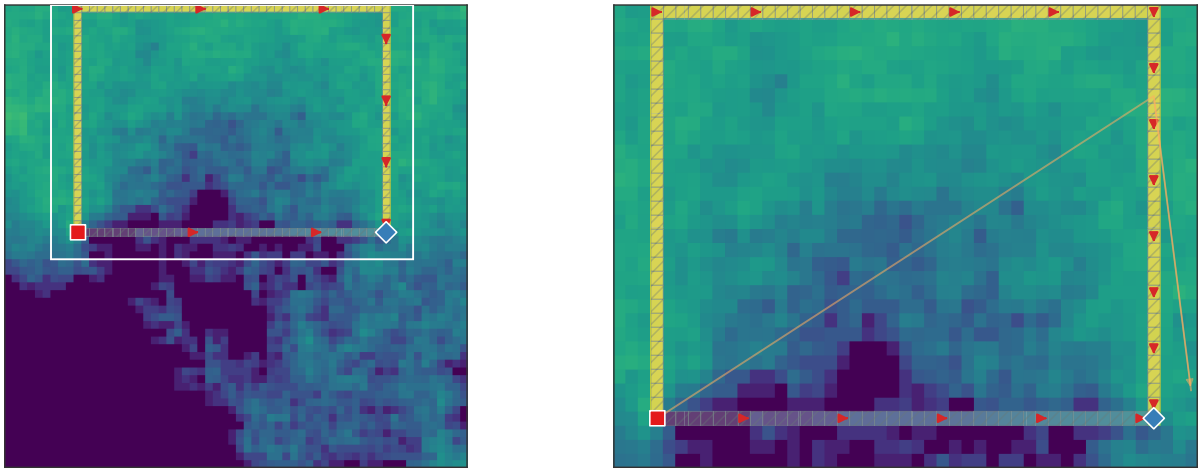


Figure 54: S1: slow-channel path density + representative paths (full + ROI).

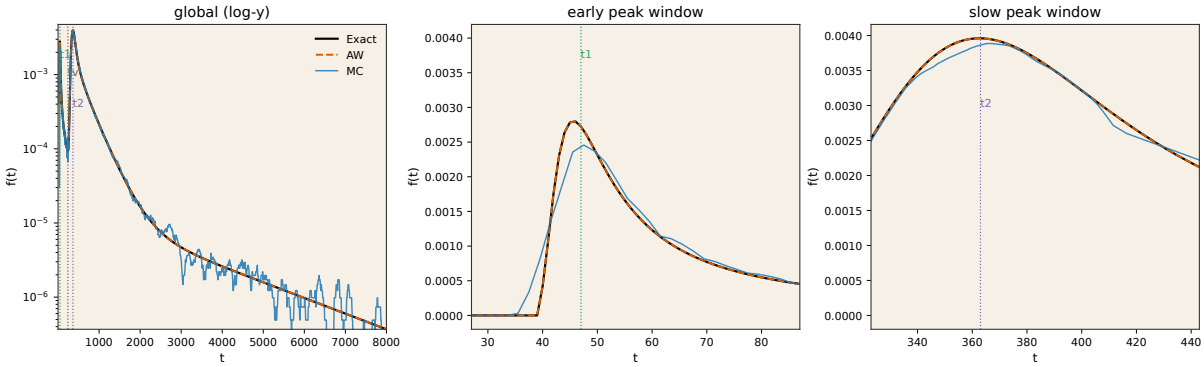


Figure 55: S1: multiscale FPT plot (Exact/AW/MC overlay).

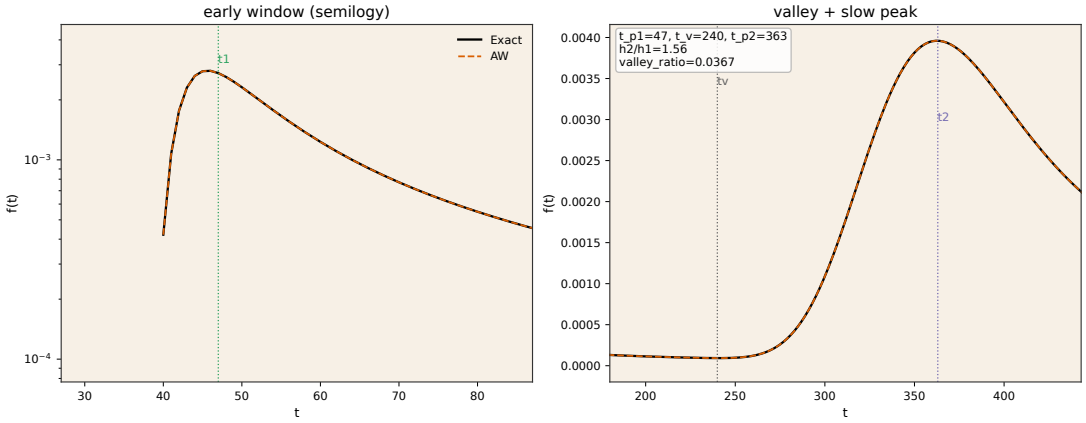


Figure 56: S1: peak–valley zoom.

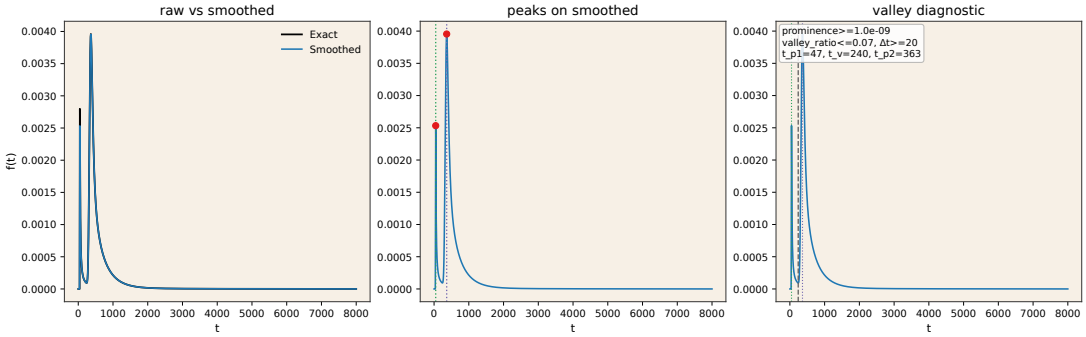


Figure 57: S1: bimodality diagnostic.

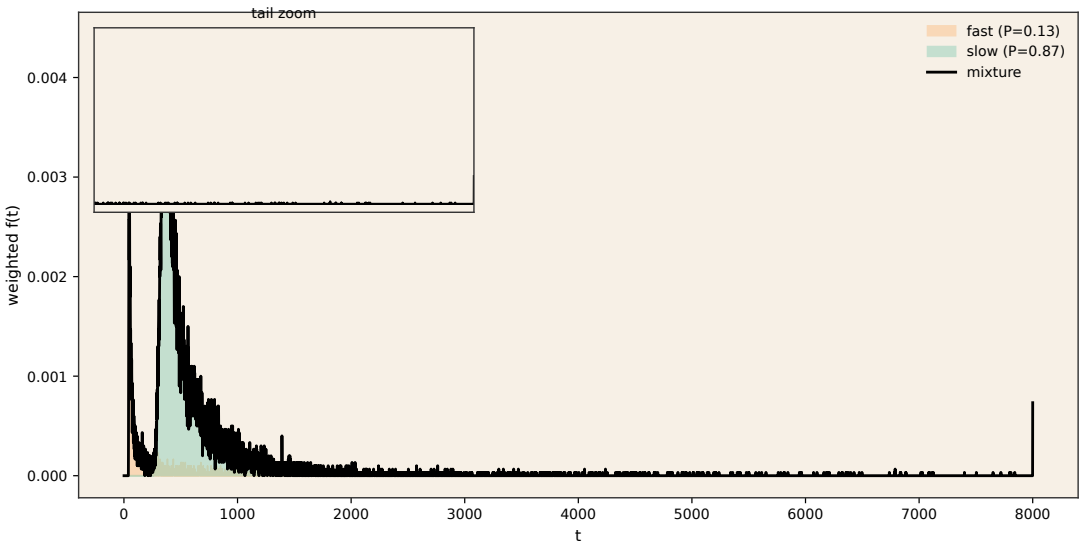


Figure 58: S1: channel decomposition and mixture.

6.8 S2: soft two-track construction (turn at $y = 10$)

S2 moves the detour turn to $y = 10$ to create a more interior soft corridor while keeping zero internal barriers/doors.

Configuration Card $N = 60,\ q = 0.8,\ g = (0, 0)$ with reflecting boundaries; start=(10,30), target=(50,30). The fast lane is $y = 30,\ x = 11..49$ with sticky factor 0.05 and rightward bias $\delta = 0.95$. The slow lane follows the left column $x = 10,\ y = 11..30$ (up), the middle edge $y = 10,\ x = 10..49$ (right), and the right column $x = 50,\ y = 10..29$ (down), again with sticky factor 0.05 and weaker bias $\delta = 0.20$. The channel rule marks any hit of the $y = 10$ segment before absorption as slow; otherwise it is fast. Metrics: $t_{p1} = 48,\ t_v = 274,\ t_{p2} = 462$; peak ratio= 0.647; valley ratio= 0.061; $P_{\text{fast}} = 0.171$.

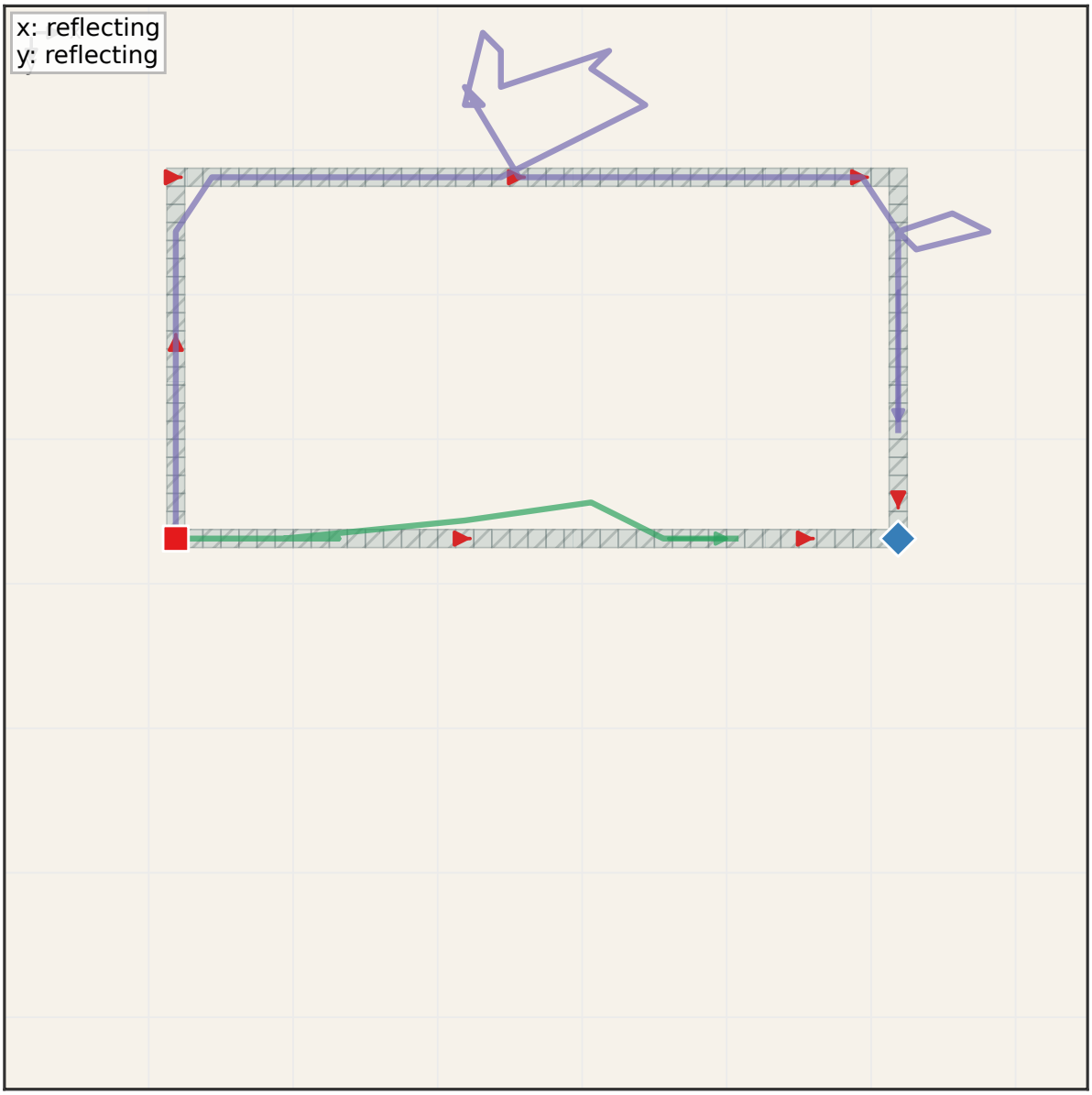


Figure 59: S2: environment schematic.

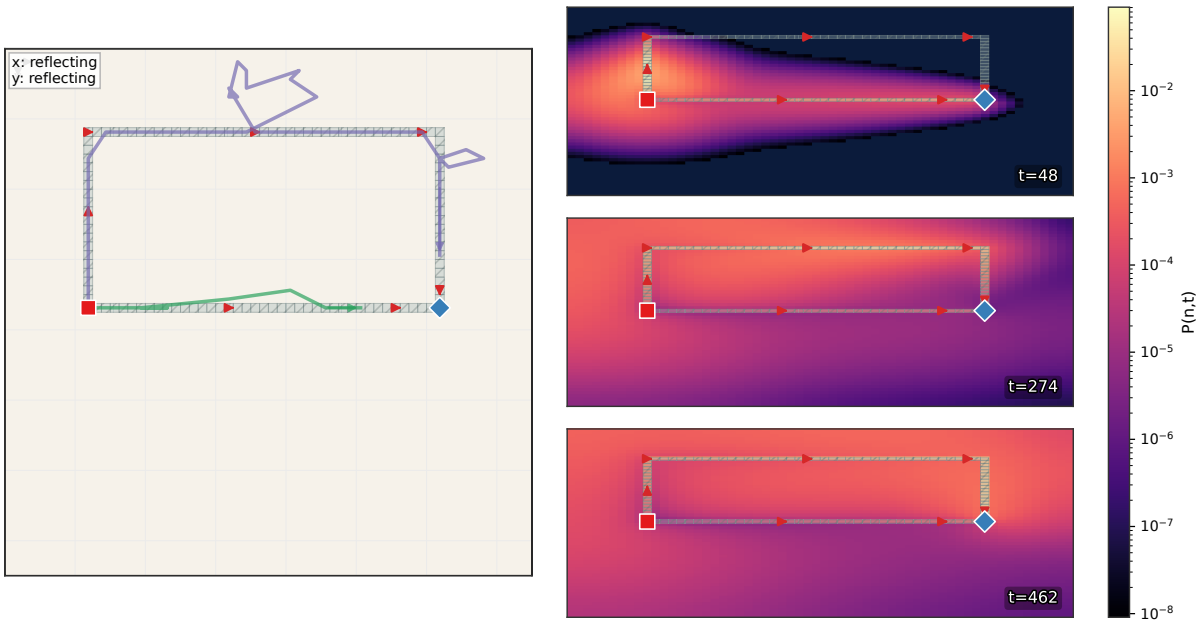


Figure 60: S2: environment and $P(n,t)$ slices at t_{p1}, t_v, t_{p2}.

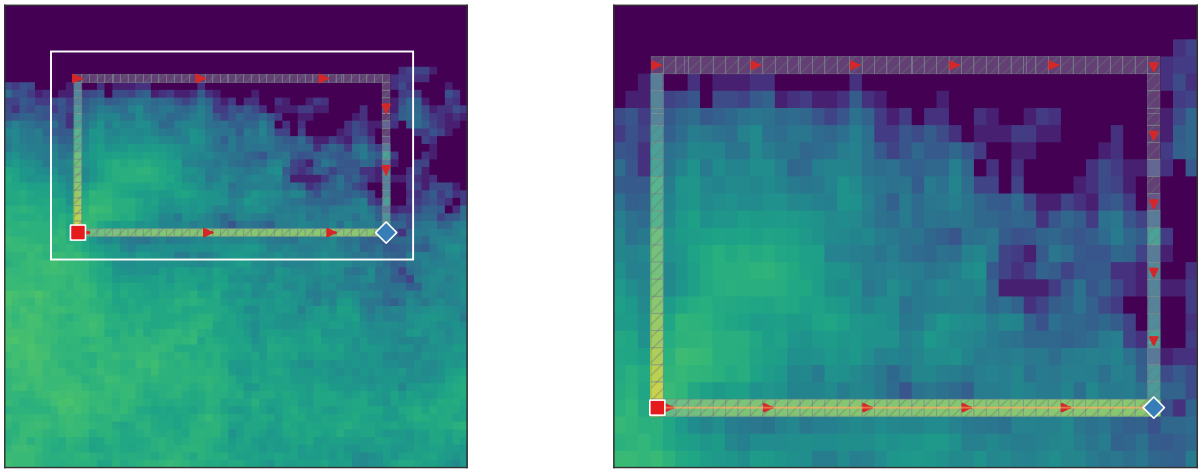


Figure 61: S2: fast-channel path density + representative paths (full + ROI).

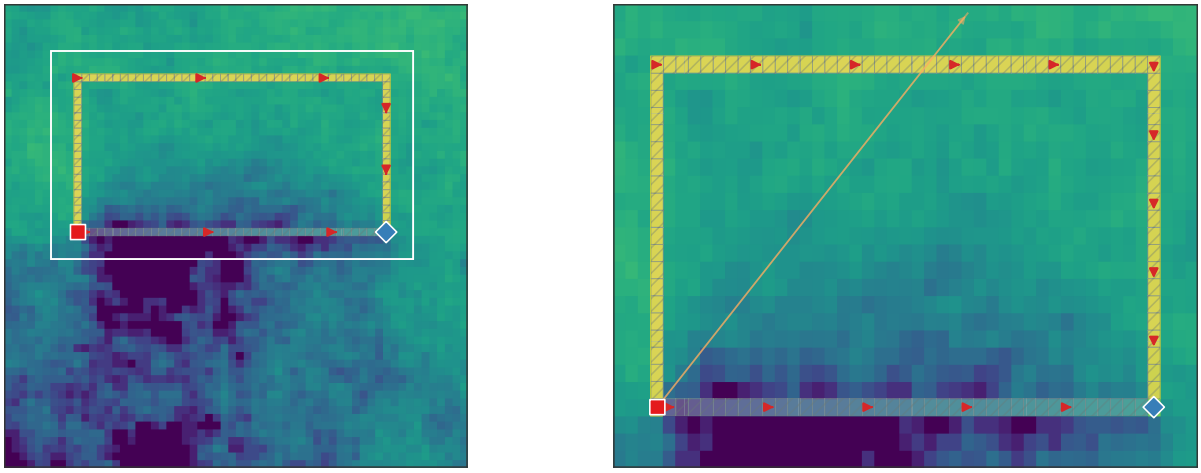


Figure 62: S2: slow-channel path density + representative paths (full + ROI).

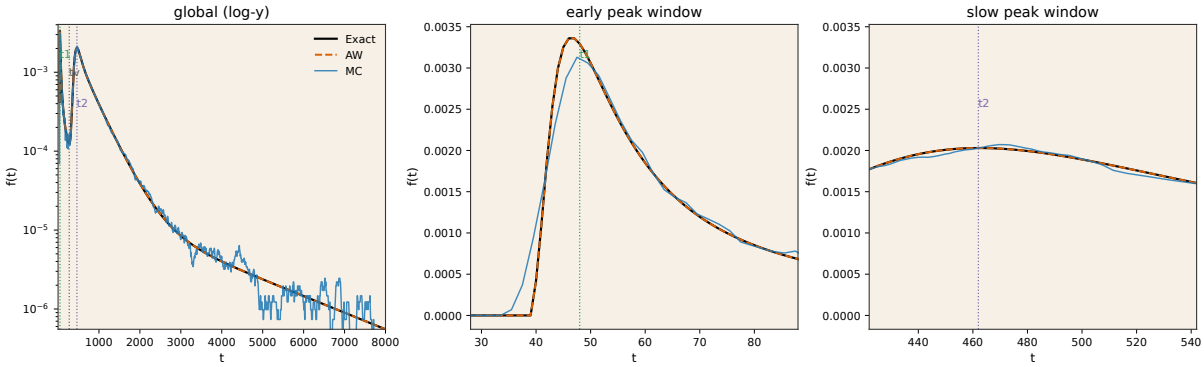


Figure 63: S2: multiscale FPT plot (Exact/AW/MC overlay).

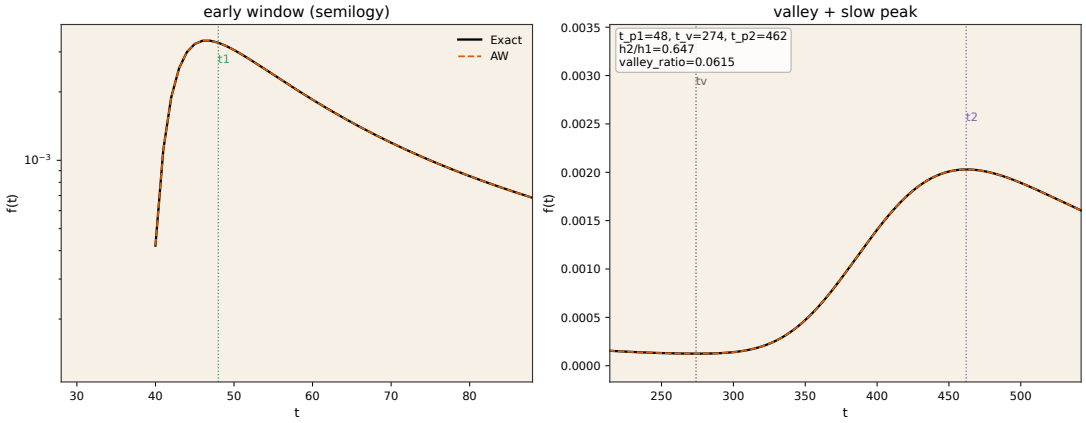


Figure 64: S2: peak–valley zoom.

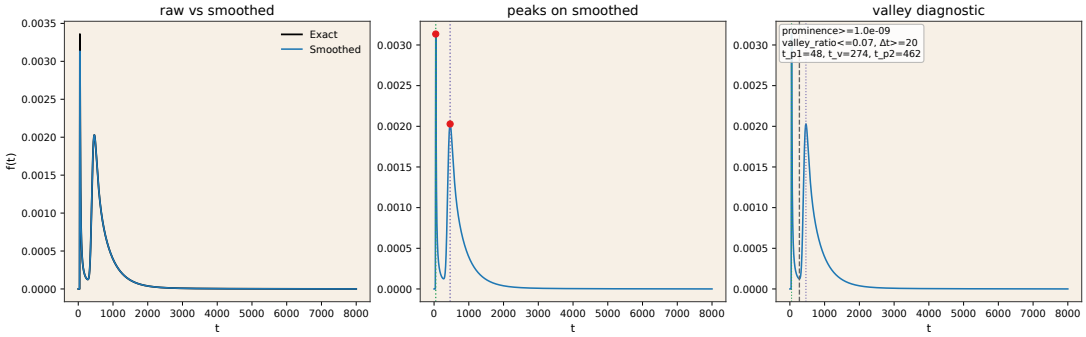


Figure 65: S2: bimodality diagnostic.

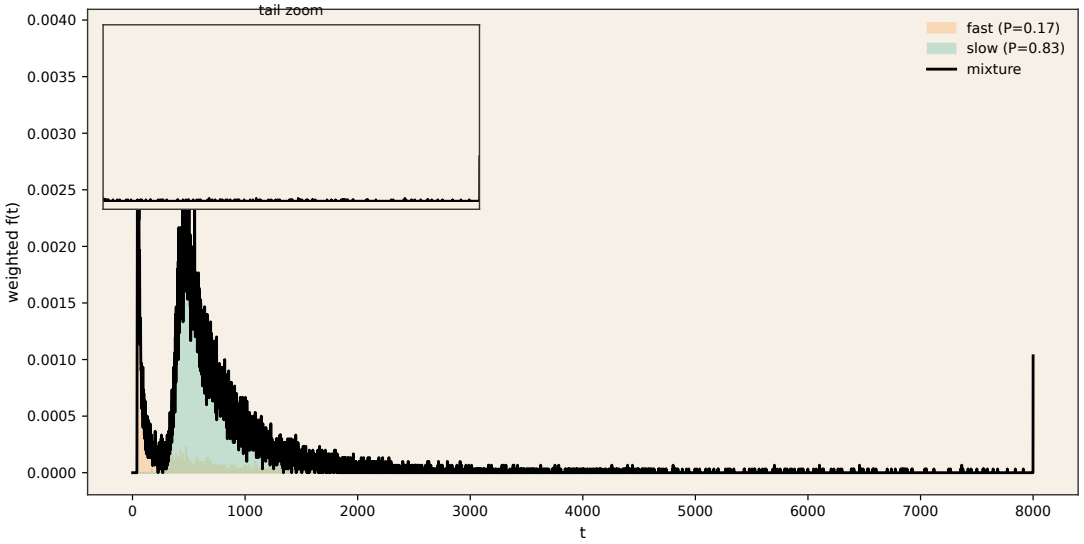


Figure 66: S2: channel decomposition and mixture.

7 Intuitive mechanism: two-channel mixture + time-scale separation

Classifying trajectories by channel event $C \in \{\text{fast}, \text{slow}\}$ gives

$$f(t) = \mathbb{P}(C = \text{fast})\, f(t \,|\, C = \text{fast}) + \mathbb{P}(C = \text{slow})\, f(t \,|\, C = \text{slow}). \tag{28}$$

When $t_{\text{fast}} \ll t_{\text{slow}}$ and $\mathbb{P}(C = \text{fast})$ is not too small, a clear valley appears between the two peaks.

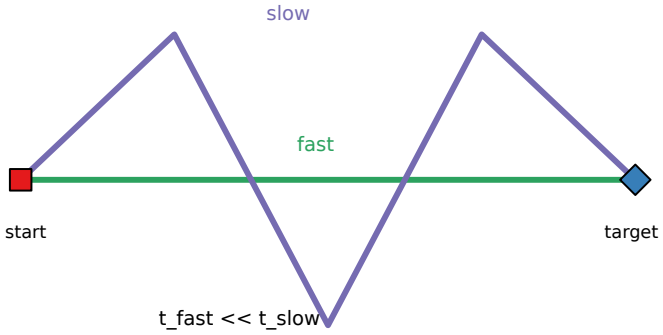


Figure 67: Conceptual sketch: bimodality as a mixture of fast/slow channels with separated time scales.

Channel criteria (fast/slow classification)

- R1: remaining on the main corridor ($y = 30$) is fast; entering the U-shaped detour is slow.
- R7: remaining on the main corridor ($y = 30$) is fast; entering the detour branch is slow.
- C3: staying on the $y = 29$ active track is fast; entering the detour loop is slow.
- R6: trajectories dominated by the $y = 20$ lane are fast; those using the $y = 40$ door lane are slow.
- NB4: no visit to the top boundary $y = 1$ before absorption is fast; any visit is slow.
- NB5: same criterion as NB4; the global bias shifts the fast/slow weights and peak locations.
- S1: no visit to the top edge $y = 1$ segment is fast; any visit is slow (soft detour).
- S2: no visit to the $y = 10$ segment is fast; any visit is slow (interior soft detour).

Geometric vs dynamical explanations

- R1: reflecting walls squeeze the space into quasi-1D corridors; short corridors are fast and long detours are slow.
- R7: a single semipermeable door provides a shortcut while the U-shaped branch creates a longer geometric detour.
- C3: a strong local-bias transport track creates the fast channel, while a long loop yields the slow channel.
- R6: the door array reduces effective throughput on the slow lane, creating a dynamical bottleneck.
- NB4: a clockwise boundary belt produces a short counterflow route and a long clockwise loop, yielding a deep valley.
- NB5: adding global drift to the boundary belt further biases the clockwise loop, deepening the valley.
- S1/S2: sticky suppresses lateral escape while local bias redirects stay probability, yielding quasi-1D soft corridors and clean fast/slow separation without internal walls.

Rough peak prediction Approximate drift along the corridor as $v \approx p_{\text{forward}} - p_{\text{backward}}$, giving $t_{\text{pred}} \approx L/v$ (order-of-magnitude intuition). Table 6 compares this estimate with the numerical peaks for the corridor/door cases; NB4/NB5 are boundary-ring drifts and are not included in this corridor approximation.

case	channel	L_{geom}	t_{pred}	t_{peak}
R1	fast	40	148	136
R1	slow	98	453	424
R7	fast	40	148	140
R7	slow	98	453	428
C3	fast	40	160	160
C3	slow	100	746	702
R6	fast	60	377	347
R6	slow	60 + door	2272	2160

Table 6: Rough peak prediction (1D drift approximation) vs numerical peak times.

R1/R7/C3 match the geometric estimate in scale; deviations for R6 come from door-induced waiting times.

8 Boundary condition note

reflecting corresponds to diffusion/search in a confined domain: probability is conserved and does not leak out. This report focuses on reflecting boundaries to show that bimodality does not require periodic topology.

9 Links to references

- PhysRevE 102, 062124: bimodality via channel mixing (explicitly in 1D), motivating the reflecting-corridor constructions.
- arXiv:2311.00464v2 (Giuggioli et al., 2024, Fig.3): construction rules for permeable barriers and sticky sites used in R6/R7/NB4/NB5.

10 Data and code availability

All scripts and data are organized in `reports/grid2d_reflecting_bimodality/`. Figures are under `figures/`, and numerical metrics/intermediate outputs are stored in `data/` and `outputs/`.

The PDF is produced via LaTeX. To reproduce, run the main script and follow the directory structure above.

References

[1] S. Sarvaharman and L. Giuggioli, *Phys. Rev. E* **102**, 062124 (2020). DOI: 10.1103/PhysRevE.102.062124.

[2] L. Giuggioli, S. Sarvaharman, D. Das, D. Marris, and T. Kay, *Multi-target search in bounded and heterogeneous environments: a lattice random walk perspective*, arXiv:2311.00464v2 [cond-mat.stat-mech] (11 Sep 2024).